

Article

# Corrosion Behavior of 2205 Duplex Stainless Steels in HCl Solution Containing Sulfide

Junlei Tang <sup>1</sup> , Xi Yang <sup>1</sup>, Yingying Wang <sup>1</sup>, Hu Wang <sup>2,\*</sup>, Ying Xiao <sup>1</sup>, Mihai Apreutesei <sup>1</sup>, Zhen Nie <sup>3</sup> and Bernard Normand <sup>4</sup> 

<sup>1</sup> School of Chemistry and Chemical Engineering, Southwest Petroleum University, Chengdu 610500, China; tangjunlei@126.com (J.T.); costeyangxi@163.com (X.Y.); yingyingwanglyon@126.com (Y.W.); xiaoyingswpu@126.com (Y.X.); mihai.projects@gmail.com (M.A.)

<sup>2</sup> School of Material Science and Engineering, Southwest Petroleum University, Chengdu 610500, China

<sup>3</sup> Research Institute of Petroleum Exploration and Development, China National Petroleum Corporation, Beijing 100083, China; niezhen@petrochina.com.cn

<sup>4</sup> MATEIS UMR CNRS 5510, INSA Lyon, Université de Lyon, 69621 Villeurbanne CEDEX, France; bernard.normand@insa-lyon.fr

\* Correspondence: senty78@126.com; Tel.: +86-028-8303-7360

Received: 26 December 2018; Accepted: 26 February 2019; Published: 5 March 2019



**Abstract:** The corrosion behavior of 2205 DSS in HCl solutions containing sulfide were investigated using mass loss test, electrochemical measurements, scanning Kelvin probe, scanning electron microscope (SEM) and X-ray photoelectron spectroscopy (XPS). The results showed that Na<sub>2</sub>S had significant effect on corrosion behavior of 2205 DSS in dilute HCl solutions. Slight Na<sub>2</sub>S can prevent the passive film from localized attacking of Cl<sup>-</sup> in HCl solution with a concentration lower than 0.1 mol/L. However, when the concentration of HCl solution higher than 0.137 mol/L, Na<sub>2</sub>S addition will tremendously promote corrosion. The intergranular corrosion combined surficial active dissolution of 2205 DSS could happen in HCl + Na<sub>2</sub>S solution.

**Keywords:** duplex stainless steel; hydrochloric acid; sulfide; EIS; XPS

## 1. Introduction

In oil and gas production and refining industries, the 2205 duplex stainless steels (DSS) as a promising material is widely used due to its excellent mechanical behavior and high corrosion resistance [1–3]. However, some severe corrosion cases of 2205 DSS occurred in such industries recently. Firstly, the corrosion situation was worsened with the increasing of quantity of sulfide, chloride and carbon dioxide in crude oil [4,5]. Secondly, in the atmospheric distillation columns and overhead condensation systems of refinery, the primary equipment directly undergo the corrosion risk from the concentrated detrimental contains (i.e., chloride and sulfide) in crude oils even after the desalting and dehydration processes [6,7]. In such systems, acidic corrosion occurred due to the combined action of hydrochloric acid and hydrogen sulfide contained [8–11]. The hydrochloric acid was formed by the hydrolysis of chlorine salt or organic chloride at high temperature, and finally became aqueous solution under dew point temperature.

The effect of single chloride or sulfide on corrosion of DSS has attracted many attentions [12–17] because both of them can affect the stability of passive metal significantly. For instance, Jeon et al. [12] focused their study on pitting corrosion of DSS in NaCl and NaCl + HCl solutions. They demonstrated that super DSS in NaCl solution of pH 7 showing pitting corrosion and in NaCl + HCl solution of pH 1 showed both uniform and pitting corrosion. It was also revealed that the ferrite phase was corroded more than the austenite phase due to different corrosion resistances in chloride solutions.

Wan et al. [13] proved that  $\text{Cl}^-$  had a strong effect on cavitation corrosion of DSS by promoting preferential dissolution of ferrous oxides and reducing the ability of passive film. In other study, Dong and Luo et al. [14] reported the pitting corrosion behavior of 2205 DSS in chloride solutions. They showed that the temperature and the concentration of chloride played important roles in changing the thickness of passive film and the shape of pits. Lo et al. [15] studied the selective dissolution of 2205 DSS between two phases, the result is that with increasing concentration of HCl, austenite phase dissolution was more faster than ferrite phase dissolution. Besides, the stress corrosion cracking in sulfur-contained condition has been investigated, for instance by Liu et al. [16] who studied the stress corrosion cracking of 2205 DSS in  $\text{CO}_2$ - $\text{H}_2\text{S}$  contained environment. It has been suggested that  $\text{H}_2\text{S}$  could primarily promote the reduction of  $\text{H}^+$  and the oxidation of steel to form FeS in the solution of pH lower than 3. Liu et al. [17] reported that the cathodic reaction can be accelerated in  $\text{H}_2\text{S}$ -contained solution, which led the fast break of passive film.

Researchers also probed the passive film property [18] and the passivation mechanism [19] of DSS in different acidic environments. However, the corrosion behavior of 2205 DSS in various concentrations of HCl solution with sulfide at high temperature had obtained less attention. Although some studies presented the results on the combination effect of chloride and sulfide in corrosive mediums with different pH values [20–23], such studies are mainly focused on carbon steel and austenite steels.

For the corrosive condition of hydrochloric acid plus sulfide solution with different concentration, how the combination effect of hydrochloric acid and sulfide affect the corrosion mechanism of 2205 DSS is still unknown. It is very important for probing the passivation destruction mechanism of 2205 DSS and defining the limitation of 2205 DSS in application. In the industrial aspect, the understanding of corrosion mechanism of 2205 DSS in HCl +  $\text{H}_2\text{S}$  solution which often occurs in atmospheric distillation columns and overhead condensation systems is mandatory to be further explored. Besides, there are other similar conditions that 2205 DSS may be applied in, for instance, the well casing under fracturing operation in  $\text{H}_2\text{S}$  contained reservoir in oil and gas production.

This work aims to provide an improved understanding of the corrosion micro-morphology, corrosion process, electrochemical mechanism and passivation destruction of 2205 DSS in the hydrochloric acid plus  $\text{Na}_2\text{S}$  at high temperature. The corrosion behaviors of 2205 DSS in HCl plus  $\text{Na}_2\text{S}$  solutions were comparably studied by mass loss, polarization curve, electrochemical impedance spectra (EIS), scanning Kelvin probe (SKP), scanning electron microscope (SEM) and X-ray photoelectron spectroscopy (XPS).

## 2. Experimental Part

### 2.1. Material and Mass Loss Test

The specimens of 2205 DSS used in this study were cut into 40 mm × 15 mm × 2 mm. The chemical composition (wt.%) of 2205 DSS were: C 0.03, Si 1.00, Mn 2.00, P 0.03, S 0.02, Ni 4.80, Cr 22.00, Mo 3.00, N 4.80 and balance Fe. The samples were sequentially polished up to 2000 grit SiC paper, degreased with acetone and alcohol, cleaned in water and dried in air.

The corrosion rates of 2205 DSS were calculated by mass loss test [24] after 8 h immersion at 90 °C in HCl solution with concentrations of 0.548 mol/L, 0.274 mol/L, 0.137 mol/L, 0.1 mol/L, 0.01 mol/L and 0.001 mol/L in the absence and presence of 0.385 mmol/L  $\text{Na}_2\text{S}$ . After taking out the sample, they are washed by pure water. The sample with corrosion product was immersed in the 10 wt.%  $\text{HNO}_3$  solution with addition of organic corrosion inhibitor for a short time to remove the corrosion product and protect from over etching, then cleaned, dried and re-weighed accurately. The filter paper was used to clean the surface of the samples in passivation during immersion. After each weight loss experiment, the samples were dried and weighed using an analytical balance (precision ± 0.1 mg). Three parallel experiments were carried out in all experiments to ensure the reliability of the experimental results. The mean weight loss value and the corresponding standard deviation were reported.

The result of corrosion rate  $R$  (mm/a) was calculated using the following formula:

$$R = \frac{(M_1 - M_2) \times 87600}{S \times T \times \rho} \quad (1)$$

where  $S$  (cm<sup>2</sup>),  $M_1$  (g),  $M_2$  (g),  $T$  (h) and  $\rho$  (g/cm<sup>3</sup>) represent the samples surface area, the weight of specimens before and after test, the time of test and the density of specimens respectively.

## 2.2. Electrochemical Experiments

Open circuit potential (OCP), EIS and polarization curve measurements were carried out in a conventional three-electrode cell using an electrochemical test system (CS350, CorrTest, China). The work electrode is 2205 DSS with exposed surface of 1 cm × 1 cm which was polished up to 2000 grit SiC paper. A saturated calomel electrode (SCE) was used as referenced electrode and a platinum foil electrode was used as counter electrode. All potentials were measured against SCE.

All the electrochemical experiments of 2205 DSS were measured at 90 °C in HCl solution with concentrations of 0.548 mol/L, 0.274 mol/L, 0.137 mol/L, 0.1 mol/L, 0.01 mol/L and 0.001 mol/L, in 0.1 mol/L HCl solution adding 0.385 mmol/L, 1.282 mmol/L, 3.846 mmol/L, and in 0.137 mol/L HCl solution adding 0.128 mmol/L, 0.385 mmol/L 0.385 mmol/L. These conditions are set to present the possible corrosion environments in atmospheric distillation columns, overhead condensation systems.

After one hour of OCP measurement, EIS were tested in frequency range from 100 kHz to 0.01 Hz with an AC amplitude peak to peak value of 10 mV (vs. OCP). Then, polarization curves were recorded by dynamic potential scanning starting from −0.1 V (vs. OCP) at a scanning rate of 0.5 mV/s. Three parallel experiments were carried out in all experiments to ensure the reliability of the experimental results. The impedance data were fitted with ZsimpWin software using equivalent circuits.

## 2.3. Scanning Kelvin Probe

The potential maps of 2205 DSS sample before and after immersion in 0.137 mol/L HCl + 0.385 mmol/L Na<sub>2</sub>S solution were recorded by SKP technique. The experiments were performed on electrochemical scanning system–VersaSCAN (AMETEK, San Diego, CA, USA). All tests were carried out at the same ambient temperature and relative humidity. Step scan mode was employed, with a step size of 20 μm and a scan area of 1000 μm × 1000 μm [25].

## 2.4. Morphological and Chemical Analysis

The surface morphologies of 2205 DSS samples with or without corrosion products were observed by scanning electron microscope (EVO MA15, Carl Zeiss Jena, Germany). The chemical composition of 2205 DSS surface was analyzed with X-ray photoelectron spectrometer (ESCALAB 250, Thermo Fisher Scientific, Waltham, MA, USA), using a monochromatic Al Kα 150 W as radiation source with the energy of 200 eV and a pass energy of 30 eV. The splitting and fitting of overlapped peaks were performed with the commercial software Xpspeak4.1 (Raymund Kwok, The Chinese University of Hong Kong, Hong Kong, China) which contains the Shirley background subtraction and Gaussian Lorentzian tail function for better spectra fitting.

# 3. Results

## 3.1. Mass Loss Test

Table 1 shows the corrosion rates of 2205 DSS in different concentration of HCl solution with or without 0.385 mmol/L Na<sub>2</sub>S at 90 °C for 8 h. Two vertical coordinates are presented in the Figure 1, one is corrosion rate and another is growth ratio. Growth ratio (%) was calculated using the following formula:

$$\text{Growth Ratio (\%)} = \frac{CR - CR_0}{CR_0} \times 100 \quad (2)$$

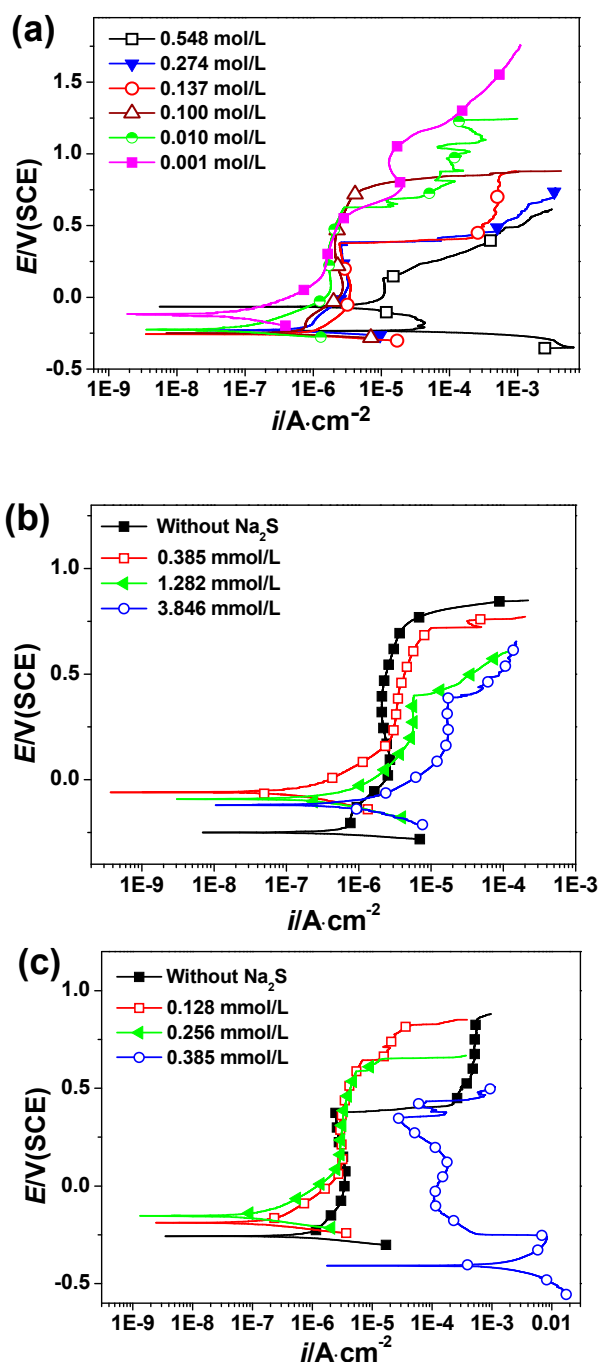


**Figure 1.** Polarization curves of 2205 DSS in (a) HCl solutions, (b) 0.1 mol/L HCl + Na<sub>2</sub>S solutions and (c) 0.137 mol/L HCl + Na<sub>2</sub>S solutions at 90 °C.

$CR$  and  $CR_0$  represent corrosion rates of the samples between presence and absence of 0.385 mmol/L Na<sub>2</sub>S. The corrosion rate is slightly reduced in HCl concentration below 0.137 mol/L by Na<sub>2</sub>S addition, indicating that Na<sub>2</sub>S has an inhibition effect in HCl solutions of lower concentration. In 0.137 mol/L and 0.274 mol/L HCl concentrations without Na<sub>2</sub>S, the corrosion rates are 0.0114 mm/a and 0.0130 mm/a, respectively. However, the presence of 0.385 mmol/L Na<sub>2</sub>S makes the corrosion rates of 2205 DSS grow up to 12.364 mm/a and 24.506 mm/a respectively in 0.137 mol/L and 0.274 mol/L HCl solutions. Moreover, the corrosion rate growth ratios increase to 108,549% and 188,551% accordingly. As 2205 DSS presents an active dissolution, the corrosion rates in 0.548 mol/L HCl with and without Na<sub>2</sub>S, rise to 52.734 mm/a and 81.252 mm/a respectively, while growth ratio declines to 54%.

The results presented in Table 1 shows that by adding Na<sub>2</sub>S, the critical HCl concentration for active dissolution corrosion of 2205 DSS reduces from 0.548 mol/L to 0.137 mol/L.

**Table 1.** Corrosion rates of 2205 DSS in different concentrations of HCl solution with or without Na<sub>2</sub>S at 90 °C.

$C_{HCl}$ (mol/L)	Corrosion Rate without Na <sub>2</sub> S (mm/a)	$X_1^2$	Corrosion Rate with 0.385 mmol/L Na <sub>2</sub> S (mm/a)	$X_2^2$	Growth Ratio (%)
0.001	0.0095	$5.4 \times 10^{-2}$	0.0091	$7.6 \times 10^{-2}$	−4
0.01	0.0097	$6.9 \times 10^{-2}$	0.0093	$6.5 \times 10^{-2}$	−4
0.1	0.0113	$7.3 \times 10^{-2}$	0.0111	$6.7 \times 10^{-2}$	−2
0.137	0.0114	$6.5 \times 10^{-2}$	12.364	$2.2 \times 10^{-2}$	108,549
0.274	0.0130	$8.1 \times 10^{-2}$	24.506	$7.0 \times 10^{-2}$	188,551
0.548	52.734	$7.4 \times 10^{-2}$	81.252	$9.8 \times 10^{-3}$	54

### 3.2. Polarization Curves Measurement

Figure 1 shows polarization curves of 2205 DSS in HCl solutions without and with different concentration Na<sub>2</sub>S at 90 °C. Generally, 2205 DSS passivates spontaneously in aerated dilute HCl solution and the cathodic reaction is dissolved oxygen reduction. However, Cl<sup>−</sup> has strongly destructive effect on passive film [26,27], hence the stability of passive film of 2205 DSS would decrease. As shown in Figure 1a, the corrosion potential shifts to negative region by increasing the HCl concentration while the passivation current density increases.

On the other hand, the passive region becomes narrower and breakdown potential decreases due to increase of HCl concentration. Breakdown potential is the potential of sudden increase of current after passivation region. The first significant change can be observed at 0.137 mol/L HCl with pH 0.863, since the breakdown potential of passive film drops suddenly about 0.3 V. Because the sample is still in a passivation state, hydrogen depolarization reaction could be ignored. This indicates that 0.137 mol/L Cl<sup>−</sup> ions is the critical composition to stabilize the passive film on the 2205 DSS surface. The second important change occurs in 0.548 mol/L HCl solution with pH 0.261, in which two free corrosion potentials may be seen on the polarization curve of 2205 DSS, as previously reported [28]. It can be ascribed to an unstable state of the passivation of 2205 DSS at these concentrations in the HCl solution.

Figure 1b illustrates the polarization curves for 2205 DSS in 0.1 mol/L HCl solution (lower than critical concentration) with Na<sub>2</sub>S concentrations from 0 to 3.846 mmol/L. With the addition of Na<sub>2</sub>S, corrosion potential is shifting to more positive region, indicating that Na<sub>2</sub>S can significantly influence the cathodic reaction.

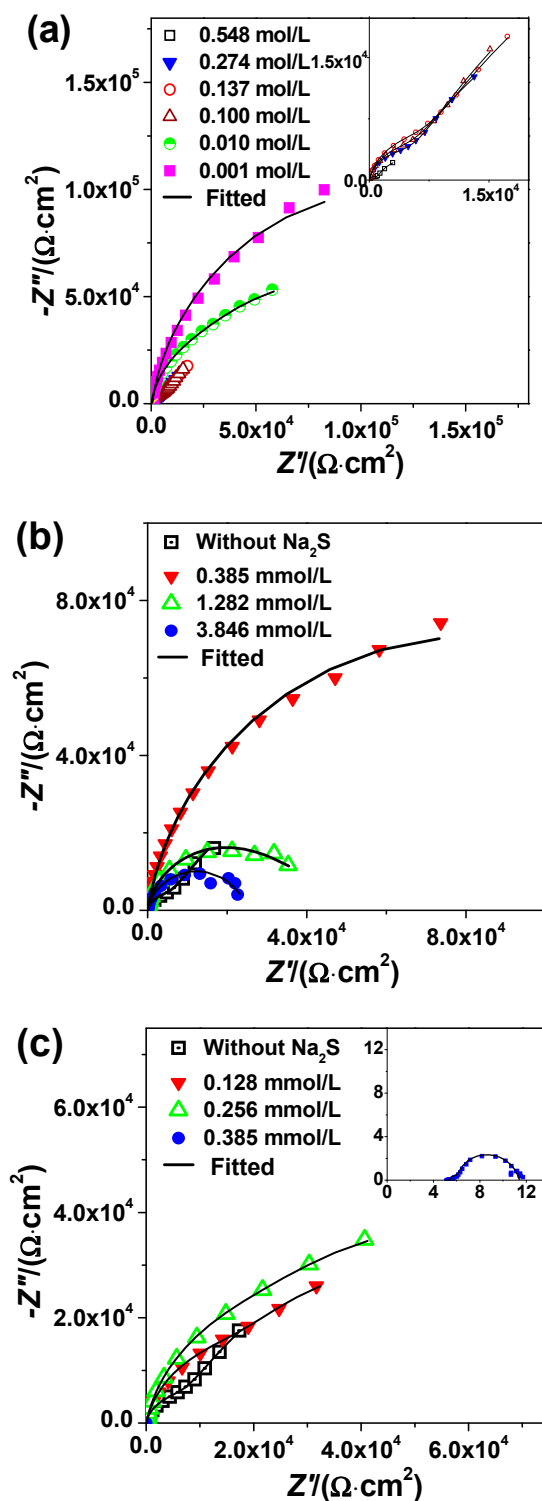
Moreover, at concentrations higher than 0.385 mmol/L the passivation current density increases, while potential decreases by increasing the Na<sub>2</sub>S concentration. One possible reason is that sulfide ion can inhibit OH<sup>−</sup> or O<sub>2</sub> and adsorb on the metal surface, hence obstructing the regeneration of passive film [29].

Figure 1c shows the polarization curves of 2205 DSS in 0.137 mol/L HCl solutions with Na<sub>2</sub>S concentration up to 0.385 mmol/L. When adding 0.128 mmol/L and 0.256 mmol/L Na<sub>2</sub>S in solution, the corrosion potential shifts to more positive direction and a wider passivation region is attained. The passivation current density remains at similar values, suggesting localized corrosion is inhibited by sulfide [30]. However, it may be seen that corrosion potential decreases rapidly and anodic current densities increased respectively when the concentration of Na<sub>2</sub>S increases to 0.385 mmol/L. Such behavior agrees with the mass loss test, implying that the corrosion process is promoted by sulfide and 2205 DSS cannot passivate anymore.

### 3.3. EIS Study

In order to understand the electrochemical kinetic at interface, Figure 2 shows the Nyquist plots based on EIS measurement after 1 h immersion. As shown in Figure 2a, when the concentration of HCl

is higher than 0.01 mol/L, Nyquist plots present double capacitive semicircle that exhibits two distinct time constants, indicating an incomplete passivation state on the surface of the 2205 DSS [31,32]. At lower HCl (0.001 and 0.01 mol/L) concentration, the capacitive semicircle extends at high frequency and the Nyquist plots became smoother, denoting a stable passive film has formed on the surface [33]. Thus, it is inferred that the corrosion resistance of 2205 DSS decreases with the increase of HCl concentration.



**Figure 2.** Nyquist plots and the fitting curves for 2205 DSS in (a) HCl solutions, (b) 0.1 mol/L HCl +  $\text{Na}_2\text{S}$  solutions and (c) 0.137 mol/L HCl +  $\text{Na}_2\text{S}$  solutions at 90 °C.

Figure 2b displays Nyquist plots of 2205 DSS in 0.1 mol/L HCl solutions with different Na<sub>2</sub>S concentrations. The capacitive semicircle of Nyquist plots becomes larger with the presence of 0.385 mmol/L Na<sub>2</sub>S, indicating an improvement of the corrosion resistance. Nevertheless, the capacitive semicircle seems to decrease with the increase of Na<sub>2</sub>S from 0.385 to 3.846 mmol/L, indicating that the corrosion resistance of 2205 DSS in HCl + Na<sub>2</sub>S solution decreases with the increase of Na<sub>2</sub>S concentration.

Figure 2c illustrates the Nyquist plots of 2205 DSS in 0.137 mol/L HCl solutions with different concentrations of Na<sub>2</sub>S. The form of capacitive semicircle of Nyquist plots is changed by adding Na<sub>2</sub>S within 0.128 and 0.256 mmol/L concentrations compared to blank solution, demonstrating that the corrosion kinetics of 2205 DSS is affected by the presence of sulfide trace. Nevertheless, when the concentration of Na<sub>2</sub>S reaches 0.385 mmol/L, the active dissolution of 2205 DSS occurs, hence the capacitive semicircle of Nyquist plots decreases suddenly. This behavior agrees with the results obtained from mass loss as well as the polarization curves (Figure 1).

On the other hand, the kinetic parameters affected by sulfide addition have been explored by using the equivalent circuit shown in Figure 3 [19] for the passive film growth stage. The circuit has two time constants. The physical interpretation of this equivalent electric circuit diagram could be interpreted as a defects-contained passive film growing on the surface of 2205 DSS in the beginning hours of immersion. The parameter constant phase element  $CPE_1$  represents the capacitive behavior of passive film. The  $R_1$  parameter defines the film resistance of growing oxide film. The constant phase element  $CPE_2$  represents the capacitive behavior,  $R_2$  for the corresponding charge-transfer resistance [34,35] of electrochemical reaction at solution/metal interface and  $R_s$  is the solution resistance. The EIS fitting results of 2205 DSS in 0.1 mol/L and 0.137 mol/L HCl solutions with different addition of Na<sub>2</sub>S are listed in Table 2.

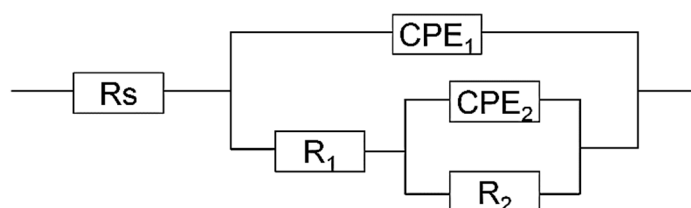


Figure 3. Equivalent circuit for EIS fitting.

Table 2. EIS fitting data of 2205 DSS in HCl solution with different Na<sub>2</sub>S at 90 °C.

HCl (mol/L)	Na <sub>2</sub> S (mmol/L)	$R_s$ ( $\Omega \cdot \text{cm}^2$ )	$CPE_1$ ( $\mu\Omega^{-1} \cdot \text{cm}^{-2} \cdot \text{s}$ )	$n_1$	$R_1$ ( $\text{K}\Omega \cdot \text{cm}^2$ )	$CPE_2$ ( $\mu\Omega^{-1} \cdot \text{cm}^{-2} \cdot \text{s}^n$ )	$n_2$	$R_2$ ( $\text{K}\Omega \cdot \text{cm}^2$ )	$X^2$
0.100	0	9.67	71.71	0.90	11.04	278.70	0.80	109.70	$2.5 \times 10^{-4}$
	0.385	7.94	62.81	0.90	13.12	4.43	0.80	155.90	$2.7 \times 10^{-4}$
	1.282	7.35	60.21	0.90	36.78	1103.00	0.80	10.60	$3.8 \times 10^{-4}$
	3.846	6.97	66.58	0.88	22.86	3746.00	0.80	1.50	$2.3 \times 10^{-4}$
0.137	0	5.99	75.61	0.89	10.79	293.3	0.80	66.74	$1.6 \times 10^{-4}$
	0.128	5.82	78.89	0.87	33.38	239.1	0.80	67.48	$5.0 \times 10^{-4}$
	0.256	5.54	80.16	0.87	53.51	203.2	0.80	61.65	$1.4 \times 10^{-4}$
	0.385	5.41	5545.00	0.80	0.0012	9038.00	0.97	0.0048	$3.3 \times 10^{-4}$

Based on the results from Table 2, the film resistance  $R_1$  seems to be improved due to the addition of Na<sub>2</sub>S in 0.1 mol/L HCl solution, revealing an enhancement of passive film. It worth noting that in 0.1 mol/L HCl solution with 0.385 mmol/L Na<sub>2</sub>S addition, the  $CPE_2$  decreases and  $R_2$  increases comparing with the results found for samples without Na<sub>2</sub>S, respectively. The results demonstrate that the corrosion of 2205 DSS can be successfully inhibited by adding minor amount of Na<sub>2</sub>S. Moreover, after adding Na<sub>2</sub>S, the  $CPE_2$  increased and  $R_2$  decreased by increasing the Na<sub>2</sub>S concentration, indicating the promotion of charge-discharge process of double layer related to anodic dissolution and cathodic reduction. If consider the total resistance ( $R_1 + R_2$ ) representing the overall

corrosion reaction resistance. It becomes higher by adding 0.385 mmol/L  $\text{Na}_2\text{S}$ . But the total resistance decreases with increasing  $\text{Na}_2\text{S}$  concentration in 0.1 mol/L HCl solution.

For 2205 DSS in 0.137 mol/L HCl solution without  $\text{Na}_2\text{S}$ ,  $R_1$  and  $R_2$  are both slightly reduced compared with the values obtained for 0.1 mol/L HCl. By adding  $\text{Na}_2\text{S}$  with a concentration from 0 to 0.256 mmol/L, the film resistance  $R_1$  rises with the increase of  $\text{Na}_2\text{S}$  concentration in 0.137 mol/L HCl and the value of  $R_2$  has no significant change. Consequently, the total resistance ( $R_1 + R_2$ ) is increased by small addition of  $\text{Na}_2\text{S}$ , which indicates the corrosion inhibition effect of  $\text{Na}_2\text{S}$  also presents in 0.137 mol/L HCl solution. It is in agreement with the result of polarization curve measurement (Figure 1c). However, in 0.137 mol/L HCl + 0.385 mmol/L  $\text{Na}_2\text{S}$  solution,  $CPE_1$  and  $CPE_2$  obviously increased, while  $R_1$  and  $R_2$  remarkably decreased, corresponding to the active dissolution of 2205 DSS.

### 3.4. Scanning Kelvin Probe Mapping

Figure 4 shows the surface potential 3D mapping of 2205 DSS surface before and after immersion in 0.137 mol/L HCl + 0.385 mmol/L  $\text{Na}_2\text{S}$  solution for 20 s. In Figure 4a, it can be seen a higher surface potential in top region and lower surface potential presenting in bottom region of original 2205 DSS surface. This may corresponds to austenite phase and ferrite phase, owing to ferrite phase is less noble in duplex stainless steel [36]. After immersion, the anodic region is much larger than before (Figure 4b), which indicates that corrosive medium has significant changed the surface state in few seconds. Meanwhile, the potential range also enlarges after immersion as presented in Table 3.

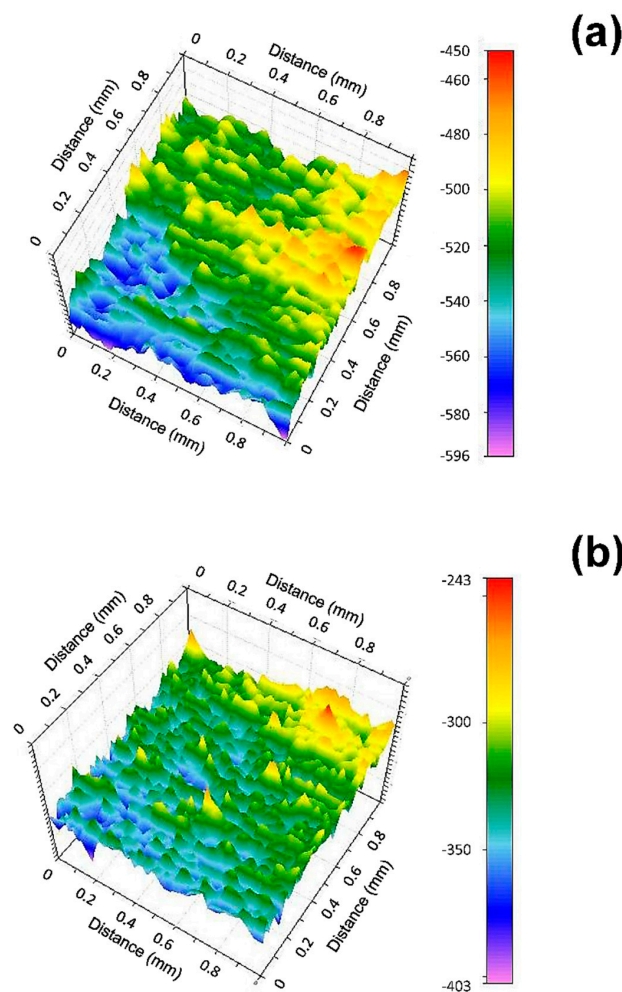


**Figure 4.** Surface potential 3D mappings of 2205 (a) before and (b) after immersion for 20 s in 0.137 mol/L HCl + 0.385 mmol/L  $\text{Na}_2\text{S}$  solution.

**Table 3.** Surface potential variation range in SKP mapping.

Samples (2205 DSS)	$\Delta E_{SKP}$ (mV)
Before immersion	146
After immersion	160

According to SKP analysis, it may be suggested that the active dissolution corrosion occurs on the most region of 2205 DSS surface from the very beginning.

### 3.5. Corrosion Micromorphology

The metallographic images of the blank sample and the corroded sample obtained by metallographic microscope are shown in Figure 5. Particularly, the blank samples were etched with solution (36 wt.% HCl: anhydrous ethanol = 1:1) in the presence of 2.5 g/L  $\text{CuCl}_2$  after polishing. In Figure 5a, the light-colored area represents the austenite phase, the fuscous area is ferrite phase. It is observed that the distribution of phases is relatively uniform. Figure 5b presents the corrosion morphology of 2205 DSS after immersion in 0.137 mol/L HCl + 0.385 mmol/L  $\text{Na}_2\text{S}$  solution. The presence of many dark areas corresponding to most corroded regions may imply that corrosion along the grain boundaries is more severe.

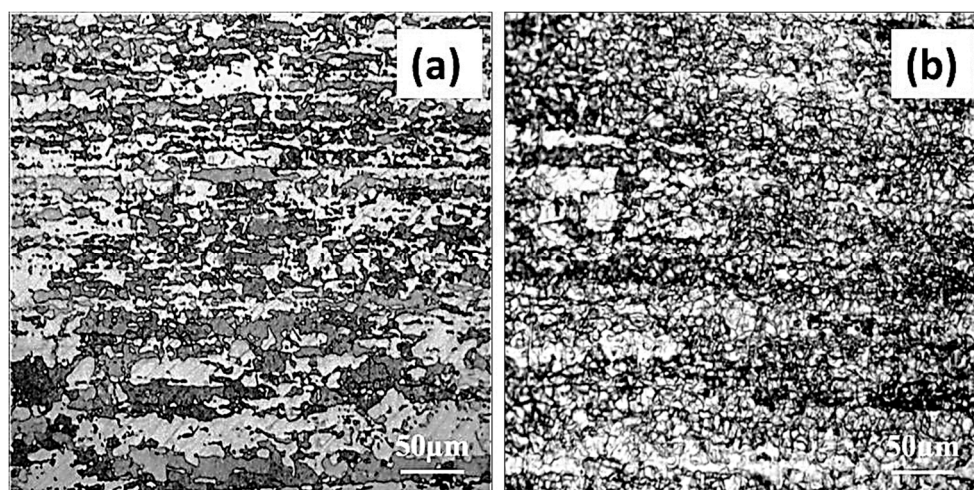


**Figure 5.** Metallographic images of 2205 DSS (a) before and (b) after 4 h of corrosion in 0.137 mol/L HCl + 0.385 mmol/L  $\text{Na}_2\text{S}$  solution, corrosion product was removed.

The SEM images of 2205 DSS after mass loss tests in HCl and HCl +  $\text{Na}_2\text{S}$  solutions are shown in Figure 6. Figure 6a reveals that 0.1 mol/L HCl solution causes pitting corrosion in local site. At higher HCl concentration (0.137 mol/L) more defects can be observed on the surface as presented in Figure 6b. These results indicate that 2205 DSS is more sensitive to localized corrosion in 0.137 mol/L HCl solution. In 0.1 mol/L HCl solution, the corrosion of 2205 DSS is retarded when added 0.385 mmol/L  $\text{Na}_2\text{S}$  (Figure 6c). Although several corrosion pits are observed in 0.1 mol/L HCl + 3.846 mmol/L  $\text{Na}_2\text{S}$ , no dramatic corrosion occurs (Figure 6d). Figure 6b,e show that 0.128 mmol/L  $\text{Na}_2\text{S}$  addition prevented the effect on the pitting corrosion of 2205 DSS in 0.137 mol/L HCl solution. However, 0.385 mmol/L  $\text{Na}_2\text{S}$  addition can cause dramatic active corrosion in 0.137 mol/L HCl solution (Figure 6f). It can be seen from the cross-section images that many corrosion defects of about 20  $\mu\text{m}$  depth are formed under the corroded layer.

The active corrosion is observed also for 0.548 mol/L HCl solution as noted from surface morphology shown in Figure 6g. In Figure 6f,g, the corrosion products covered the entire surface. Several factors may produce such fractures in the corroded layer, as for instance, the dehydration of hydroxide corrosion products and modification of  $\text{H}_2$  pathway formed by hydrogen evolution in

electrolyte/metal interface. The corresponding SEM images after removing the corrosion products from Figure 6f,g are revealed in Figure 6h,i respectively.

After the immersion of 2205 DSS in 0.137 mol/L HCl + 0.385 mmol/L Na<sub>2</sub>S solution, several micro-crack-like defects were shown in the SEM image (Figure 6h). These defects propagated deeply inside and most likely are formed at grain boundaries scale of austenite and ferrite phases. The conjunction of these defects may occur during their propagation which created the ravine-like and cave-like morphologies under the surface (Figure 6f shows their sectional view).

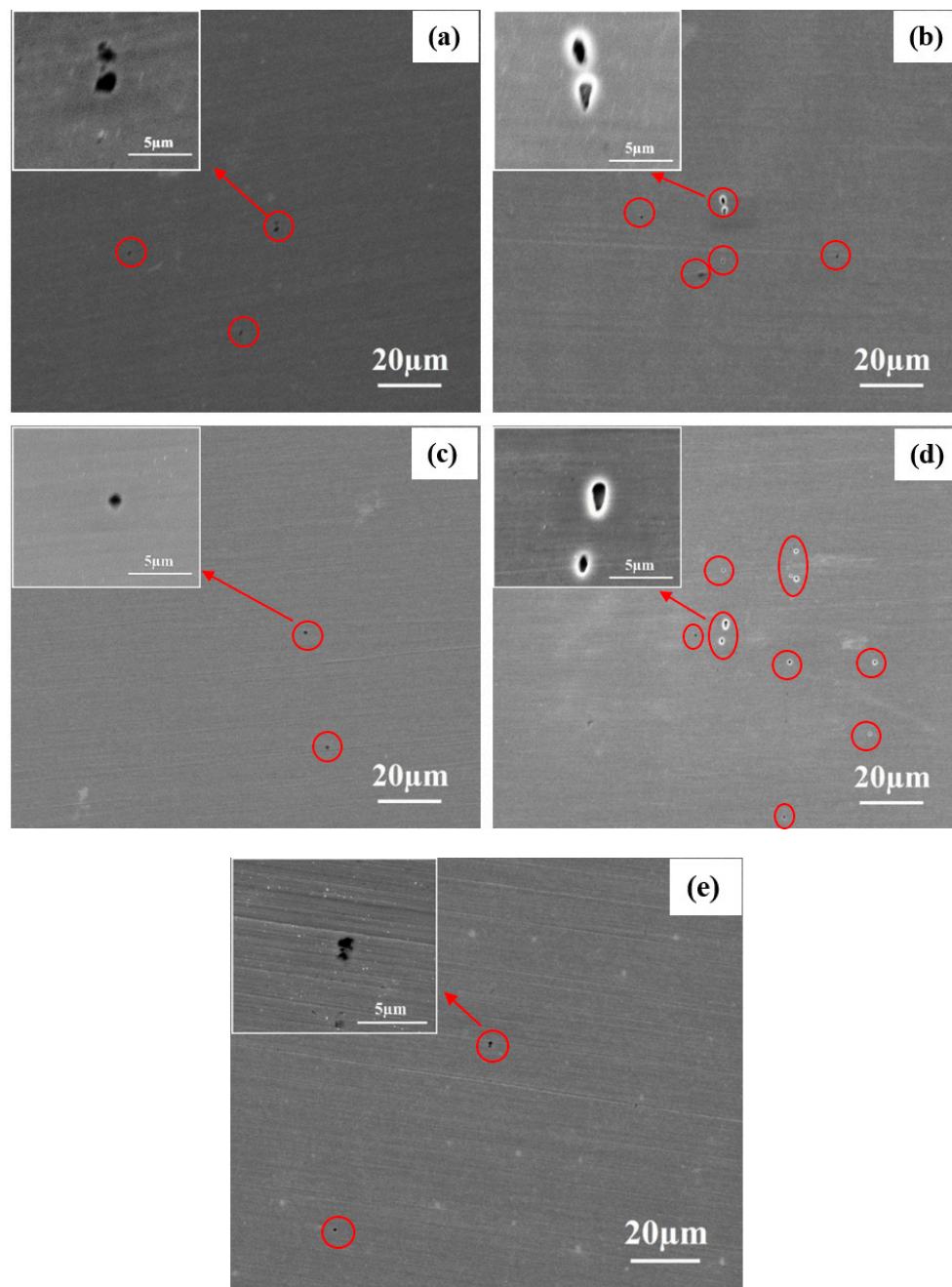
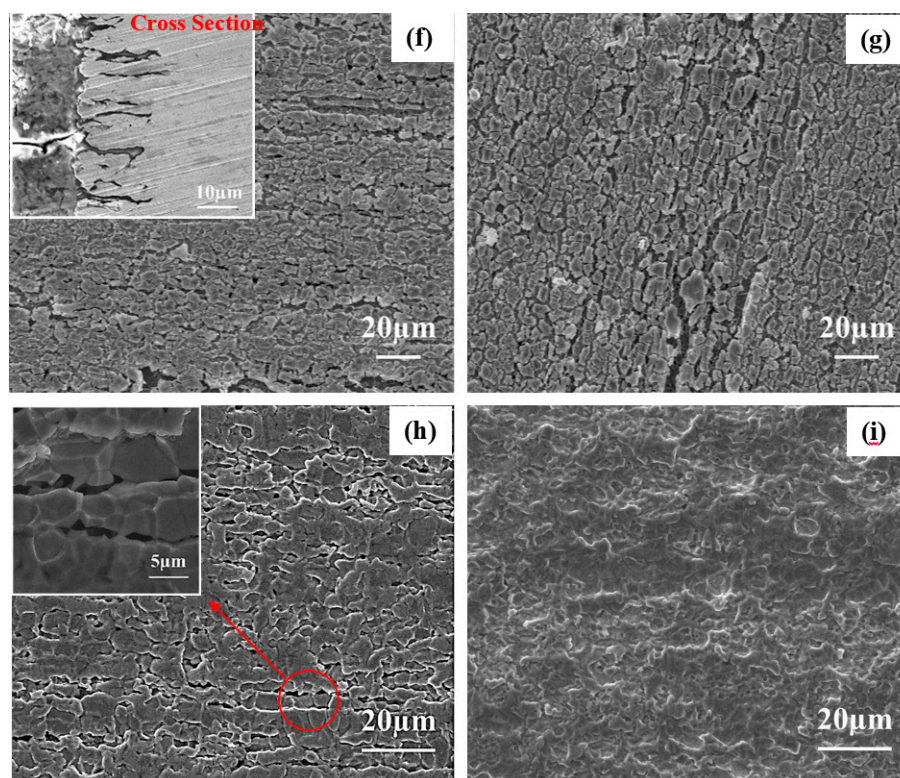


Figure 6. Cont.



**Figure 6.** Corrosion micro-morphology SEM images of 2205 DSS after 8 h of immersion in (a) 0.1 mol/L HCl, (b) 0.137 mol/L HCl, (c) 0.1 mol/L HCl + 0.385 mmol/L Na<sub>2</sub>S, (d) 0.1 mol/L HCl + 3.846 mmol/L Na<sub>2</sub>S, (e) 0.137 mol/L HCl + 0.128 mmol/L Na<sub>2</sub>S, (f) 0.137 mol/L HCl + 0.385 mmol/L Na<sub>2</sub>S, (g) 0.548 mol/L HCl, and (h) without corrosion product film 0.137 mol/L HCl + 0.385 mmol/L Na<sub>2</sub>S, (i) without corrosion product film 0.548 mol/L HCl.

On the contrast, no such defects are observed on the surface of 2205 DSS after immersion in 0.548 mol/L HCl solution without Na<sub>2</sub>S (Figure 6i). Hydrogen induced cracking (HIC) of low alloy steel or stainless steel is often found in the corrosion of H<sub>2</sub>S contained solutions [37]. Thus, a similar mechanism can be inferred for the behavior found also here for the 2205 DSS. However, these micro-cracks do not look like a typical hydrogen induced crack morphology [38] and no selective corrosion of austenite or ferrite phases has been observed according to the cross section image in Figure 6f,h. The SEM images show the remarkable feature of 2205 DSS corrosion in HCl + Na<sub>2</sub>S solution is that active dissolution happens along the grain boundaries compared to the selective dissolution of ferrite phase in H<sub>2</sub>SO<sub>4</sub>/HCl solution [39,40].

### 3.6. XPS Analysis

Figure 7 shows the general XPS spectra of passive films formed on 2205 DSS surface after immersion in 0.137 mol/L HCl and 0.137 mol/L HCl + 0.128 mmol/L Na<sub>2</sub>S solution at 90 °C for 8 h. The passive film formed on 2205 DSS surface in 137 mol/L HCl solution with 0.385 mmol/L Na<sub>2</sub>S at 90 °C for 8 h is also presented. For both two passive films, Cr, Fe, Mo, Ni and O are detected on the surface. For the corrosion product film, Cr, Mo, Ni, S, O, and some Cl traces were detected. The C 1s peaks (284.6 eV) in has been used as the reference to calibration.

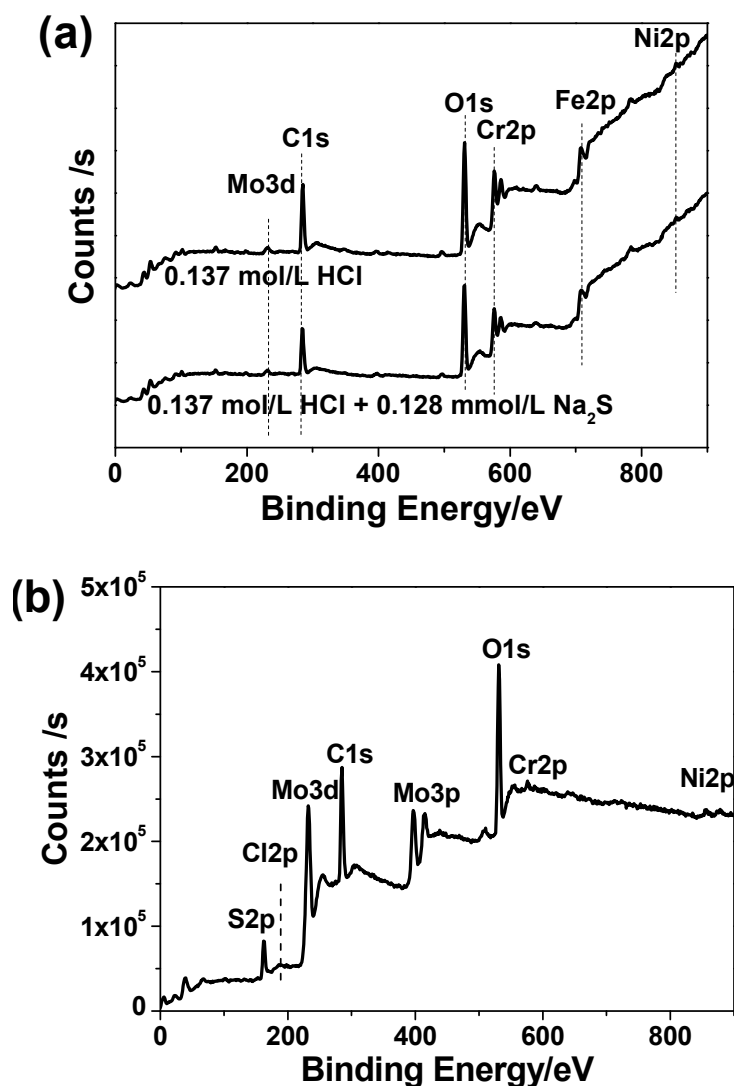


**Figure 7.** Large scale scanning XPS spectra of (a) passive films on 2205 DSS surface in 0.137 mol/L HCl solution and 0.137 mol/L HCl solution with 0.128 mmol/L  $\text{Na}_2\text{S}$ , (b) corrosion product film on 2205 DSS surface in 137 mol/L HCl solution with 0.385 mmol/L  $\text{Na}_2\text{S}$  at 90 °C for 8 h.

Figure 8 illustrates the high-resolution scanning XPS spectra for each element detected for the two passive films. It can be seen from Figure 8 that the Cr 2p spectra can be separated into several constituent peaks of metallic Cr,  $\text{Cr}_2\text{O}_3$ ,  $\text{Cr}(\text{OH})_3$ . The intensities and quantities of  $\text{Cr}_2\text{O}_3$  peaks are higher comparing to  $\text{Cr}(\text{OH})_3$  and metallic Cr, hence  $\text{Cr}_2\text{O}_3$  is the major oxide that constitutes the passive film. The Fe 2p spectra is in accordance with Fe,  $\text{Fe}_2\text{O}_3$  and  $\text{Fe}_3\text{O}_4$  metallic species. The Mo intensities are lower than others, however the overlapping peaks reveal that metallic Mo,  $\text{Mo}^{4+}$  and  $\text{Mo}^{6+}$  are present in the passive film. The Ni 2p spectrum reveals the presence of three constituent peaks representing metallic Ni and NiO. The O1s peak can be split into three components of  $\text{O}^{2-}$ ,  $\text{OH}^-$  and bound  $\text{H}_2\text{O}$ . Based on XPS analysis, it may be concluded that both passive films contain mainly oxides and hydroxides based on Cr, Mo, Ni and Fe as previously already reported [41].

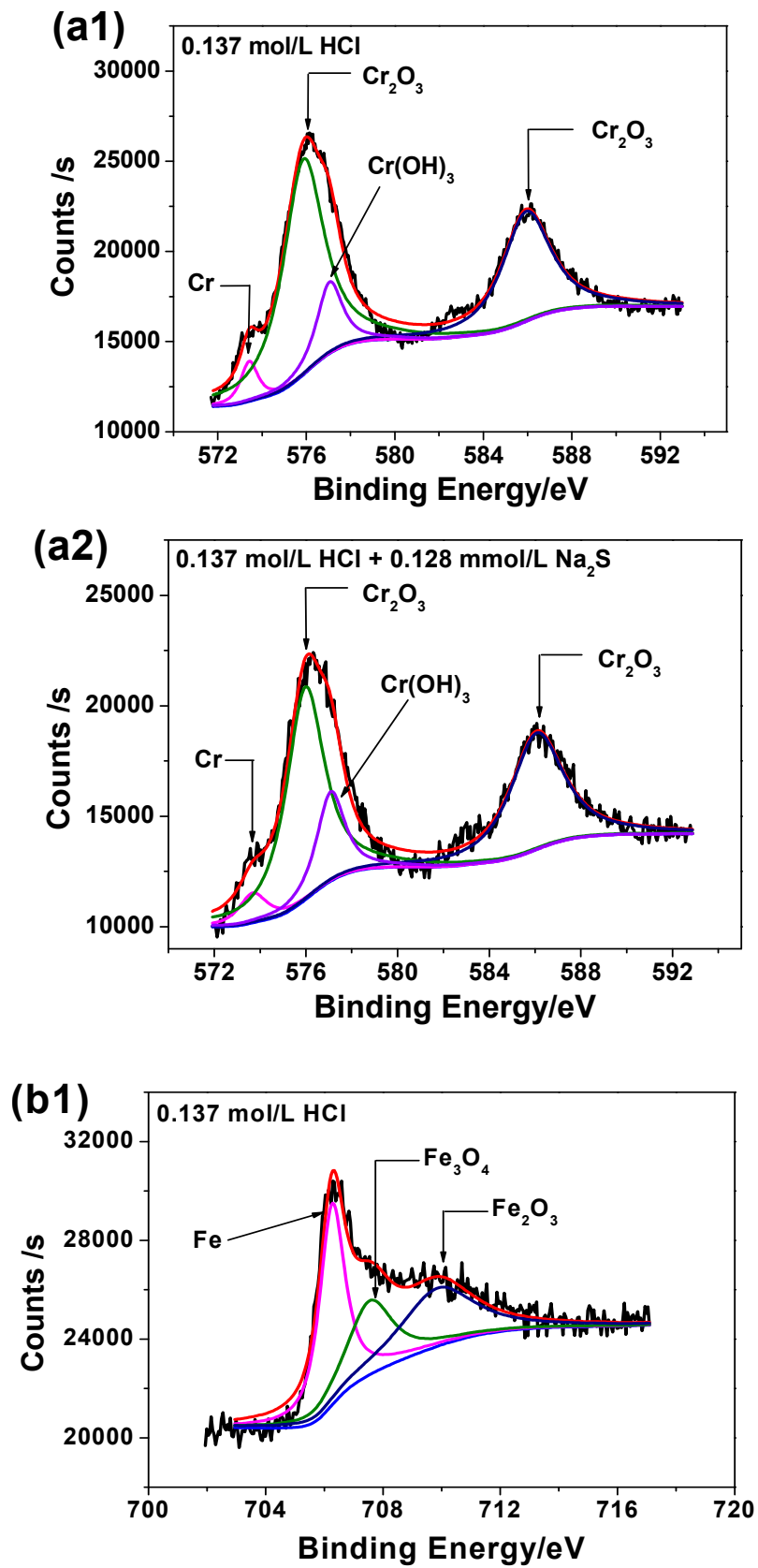


Figure 8. Cont.

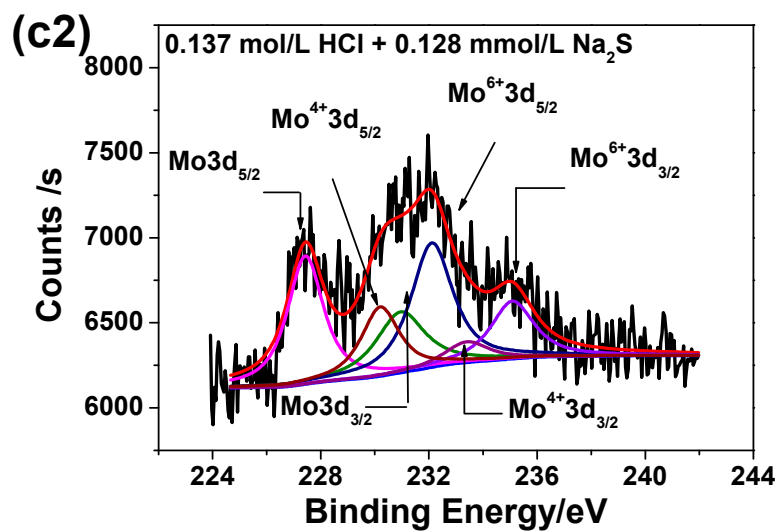
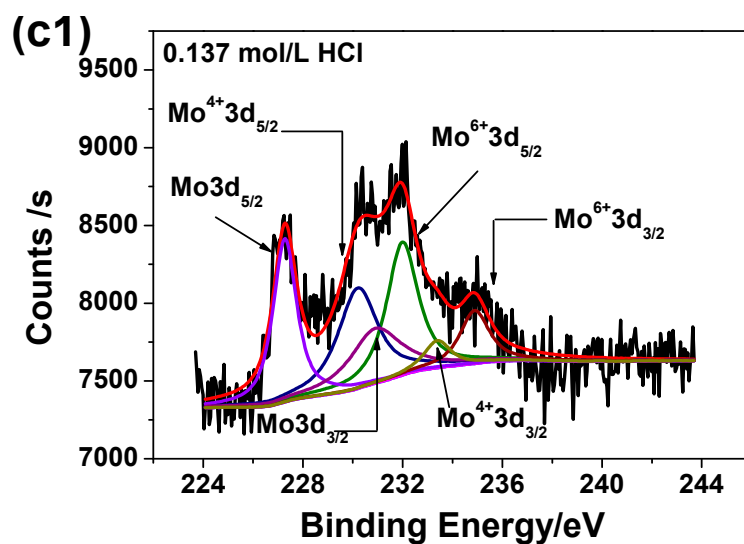
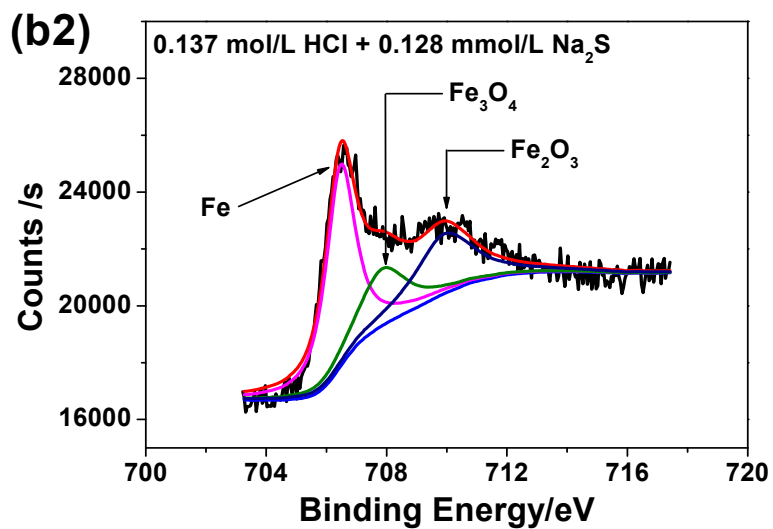


Figure 8. Cont.

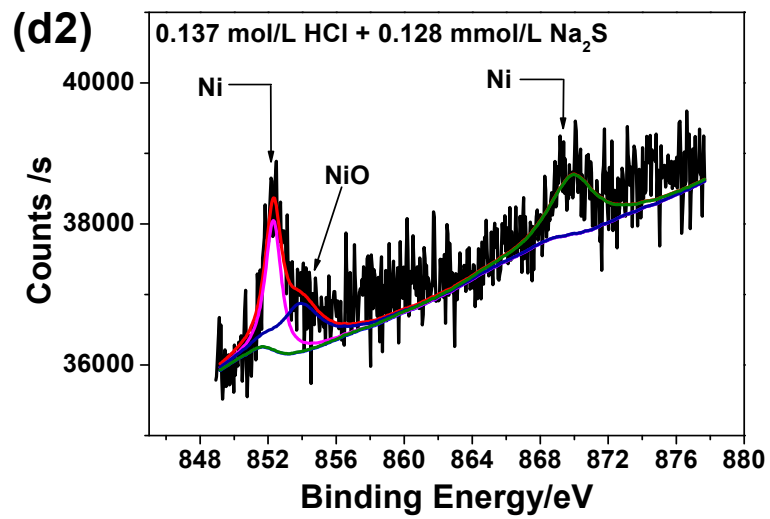
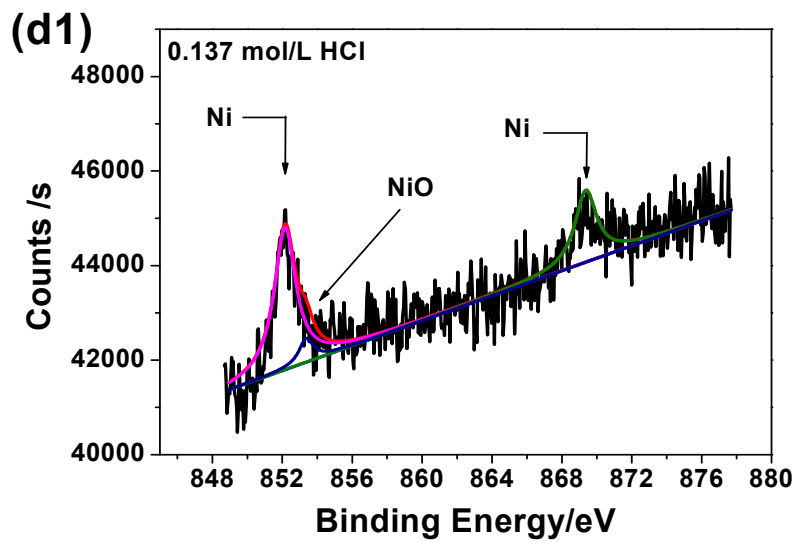
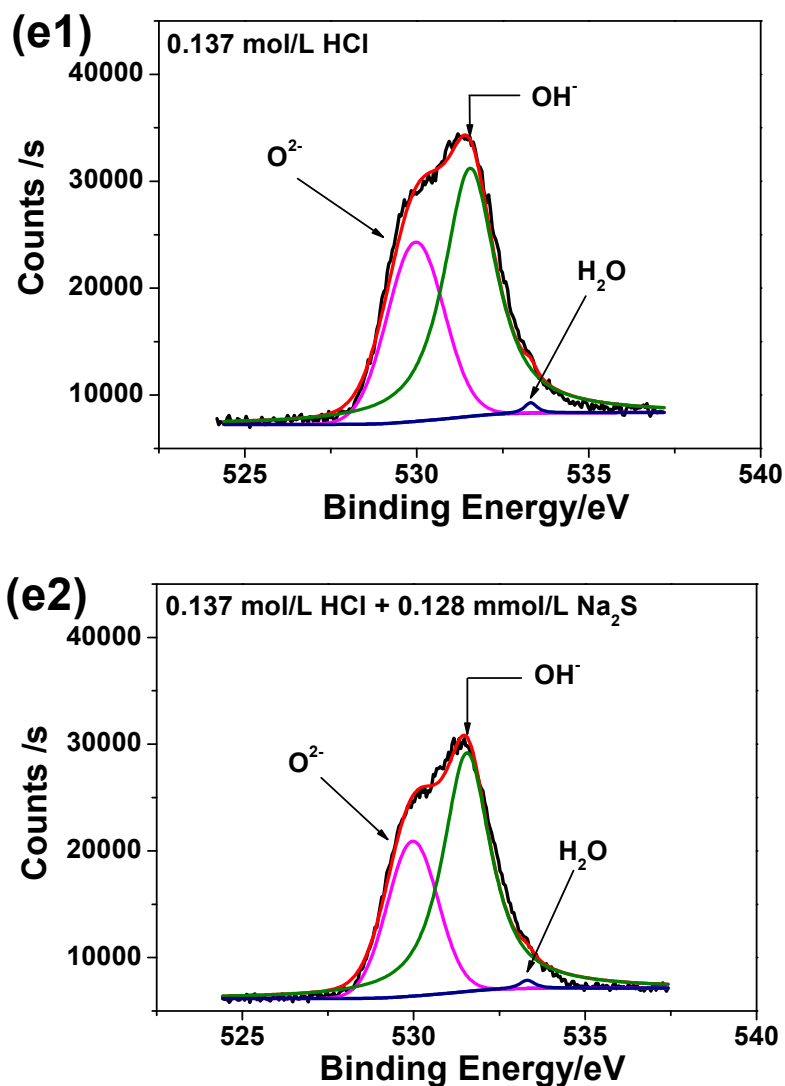


Figure 8. Cont.



**Figure 8.** High-resolution scanning XPS spectra of passive films on 2205 DSS surface in 0.137 mol/L HCl solutions at 90 °C for 8 h: (a1) Cr 2p, (a2) Cr 2p, added 0.128 mmol/L  $Na_2S$ , (b1) Fe 2p, (b2) Fe 2p, added 0.128 mmol/L  $Na_2S$ , (c1) Mo 3d, (c2) Mo 3d, added 0.128 mmol/L  $Na_2S$ , (d1) Ni 2p, (d2) Ni 2p, added 0.128 mmol/L  $Na_2S$ , (e1) O1s and (e2) O1s, added 0.128 mmol/L  $Na_2S$ .

Figure 9 shows the high-resolution scanning XPS spectra for each element found in corrosion products. The XPS peaks are separated into different combined states referring to XPS analysis of similar corrosion product [42]. The Fe 2p has been not detected and one possible explanation is that the iron can be easily dissolved into acidic solution. The peak of chromium can be deconvoluted into three peaks corresponding to  $Cr_2O_3$  and  $CrCl_3$ , as shown in Figure 9a. According to Figure 9b, high quantity of molybdenum is present in the corrosion product in form of  $Mo^{4+}$  and  $Mo^{6+}$ . Some traces of nickel have been detected as shown in Figure 9c, most likely in oxide, hydroxide and chloride form. The spectrum of S 2p shown in Figure 9d presents two constituents of  $S^{2-}$  in the corrosion products, indicating sulfide ions from  $Na_2S$  addition had taken part in corrosion reactions and different metallic sulfides were formed. The mechanism relating to sulfide ion role during the corrosion kinetics will be discussed in following section.

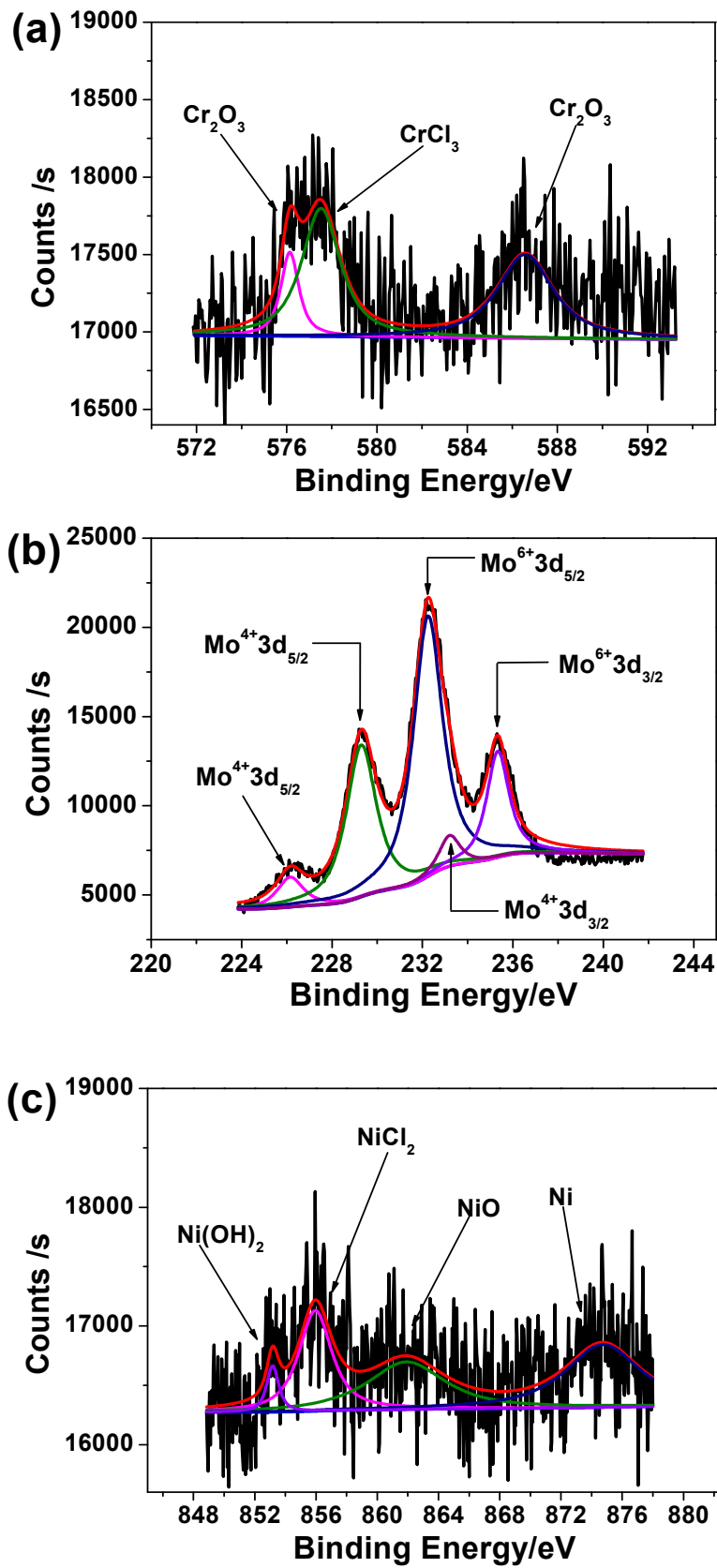
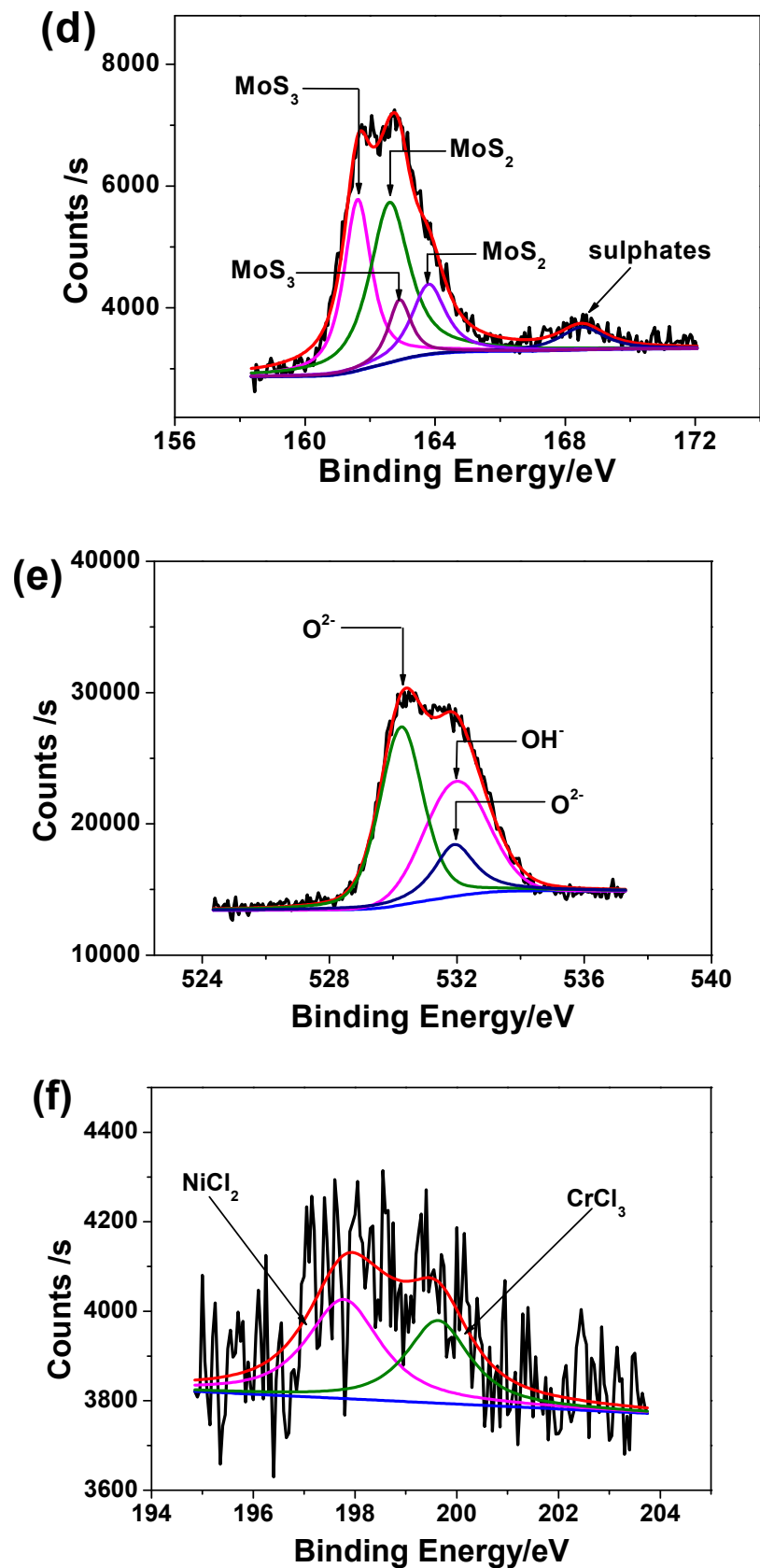
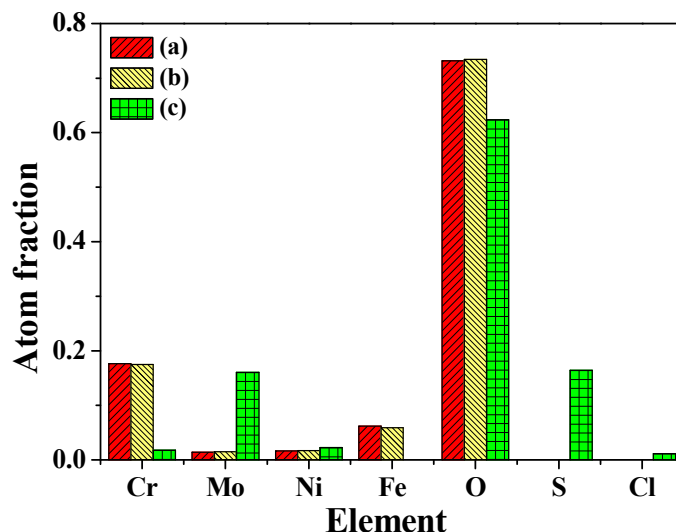


Figure 9. Cont.



**Figure 9.** High-resolution scanning XPS spectra of (a) Cr 2p, (b) Mo 3d, (c) Ni 2p, (d) S 2p, (e) O 1s and (f) Cl 2p in corrosion product film on 2205 DSS surface after immersion in 137 mol/L HCl solution with 0.385 mmol/L  $\text{Na}_2\text{S}$  at 90 °C for 8 h.

Figure 9e illustrates of O1s peaks corresponding to  $O^{2-}$  and  $OH^{-}$  that is in accordance with the presence of  $Cr_2O_3$ ,  $NiO$ ,  $Ni(OH)_2$ . The peaks of Cl 2p shown in Figure 9f correspond to  $NiCl_2$  and  $CrCl_3$ . Figure 10 shows the atom fraction for each element of 2205 DSS in superficial films under different states. No significant differences have been found for atom fractions in passive film whatever the solution composition (i.e., 0.137 mol/L HCl + 0.128 mmol/L  $Na_2S$ ).



**Figure 10.** Atom fraction of elements in surficial films of 2205 DSS: (a) passive film in 0.137 mol/L HCl solution, (b) passive film in 0.137 mol/L HCl + 0.128  $Na_2S$  solution, (c) corrosion product film in 0.137 mol/L HCl + 0.385  $Na_2S$  solution.

Nevertheless, the composition characterization of corrosion product film in 0.137 mol/L HCl + 0.385 mmol/L  $Na_2S$  solution shows that the molybdenum content increase while the chromium content decrease significantly compared with those in passive film. The molybdenum has low reactivity in hydrochloric acid (dissolution reaction) compared to other metallic elements. However, it reacts with  $H_2S$  or dissolved oxygen in acidic solution to form molybdenum sulfide, oxides and/or hydroxides, which are also stable in dilute HCl solution.

In summary, the passive film on 2205 DSS is mainly constituted of Cr(III) oxide-hydroxides with high chemical stability, which offers excellent protection of 2205 DSS matrix. In contrast, once active dissolution of 2205 DSS occurs in the solution of strong acidic and reductive properties at high temperature (the critical concentration is 0.137 mol/L HCl + 0.385 mmol/L  $Na_2S$ ), the intermediate products of ferrous oxide or sulfide would form at the interface competing with the formation of dense oxide-hydroxides. The passivation would not exist and the surficial chromium oxides would not be enough for hindering the corrosion.

#### 4. Discussion

Several micro-cracks and deep micro-holes can be seen on corroded surface of 2205 DSS in 0.137 mol/L HCl + 0.385 mmol/L based on morphology characterization by SEM (Figure 6f,h) showing intergranular corrosion which indicates that corrosion of 2205 DSS is significantly influenced by  $Na_2S$  addition.

Moreover, it is clear that the corrosion mechanism is closely associated with the role of  $Na_2S$ , which hydrolyzes easily and form  $H_2S$ ,  $HS^{-}$  and  $S^{2-}$  ions, then being preferentially absorbs on metal surface competing with  $Cl^{-}$  in hydrochloric acid solution. According to the following reaction,  $Na_2S$  is dissociated to  $H_2S$  in acidic solution [43,44]. In agreement with the pH-sulfide equilibrium diagram, at  $pH > 5.5$ , the main species is  $HS^{-}$ , otherwise it is mainly  $H_2S_{aq}$  [45,46]. The content of sodium sulfide is very low, which has little effect on the pH value in 0.1 mol/L HCl and 0.137 mol/L HCl, so the main species is  $H_2S_{aq}$ .



The adsorption mechanism on metal surface corresponding to  $\text{Na}_2\text{S}$  addition is proposed in Figure 11. As shown in Figure 11,  $\text{H}_{\text{ad}}$  represents adsorption of H on metal surface,  $\text{H}_{\text{ab}}$  represents permeation of H into the inside of metal,  $\text{H}_{\text{T}}$  is H in the trap of the metal. Meanwhile,  $\text{HS}^-$  (the main form) and  $\text{S}^{2-}$  ions have a poisoning effect on the reaction of H recombination to  $\text{H}_2$ , which increases the capacity of H on surface and promotes internal diffusion of H [21]. When the  $\text{H}_{\text{T}}$  recombines with  $\text{H}_2$ , pressure increases with the  $\text{H}_2$  aggregating in trap which causes brittleness and stress concentration. Generally is accepted that the main trapping site of steels are localized at the grain boundaries [47,48]. Duplex stainless steels have high resistance to hydrogen induced cracking in sour  $\text{H}_2\text{S}$  environments. However, the precipitation of  $\text{M}_{23}\text{C}_6$  at the  $\alpha/\gamma$  interface [49], which is associated with the carbon and chromium partitioning, may cause a dramatic deterioration in hydrogen induced corrosion resistance in acidic environments [50].

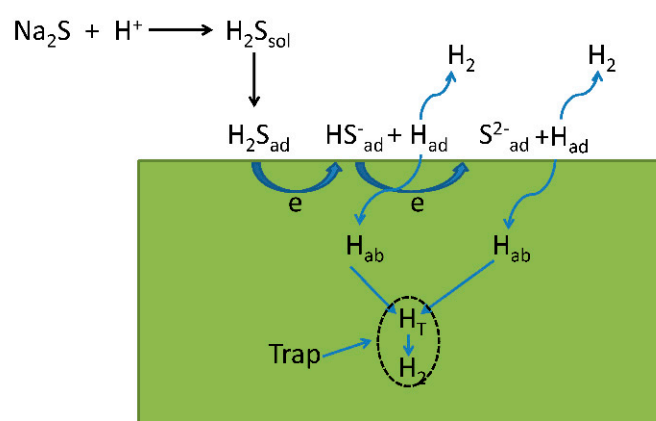


**Figure 11.** Adsorption mechanism of sulfide on metal surface.

In what concerns the 2205 DSS, the  $\text{Na}_2\text{S}$  concentration up to 3.846 mmol/L could not promote its corrosion distinctly in 0.1 mol/L HCl solution at 90 °C. However, in 0.137 mol/L HCl solution, the corrosion of 2205 DSS was extremely accelerated when  $\text{Na}_2\text{S}$  concentration reaches only 0.385 mmol/L. On the other hand, 2205 DSS has preserved a stable passivation in hydrochloric acid solution without  $\text{Na}_2\text{S}$  until the HCl concentration increases to 0.584 mol/L. Therefore, it seems that the combination effect of hydrochloric acid and sodium sulfide has two critical conditions: the first one is the HCl concentration and the second one is the sodium sulfide addition concentration. The possible corrosion mechanism of 2205 DSS investigated here is presented in Figure 12. As shown in Figure 12a, 2205 DSS keeps stable passivation in 0.1 mol/L HCl even if the passive film could be dissolved in localized area by  $\text{Cl}^-$  attacking. However, in such case the passive film of attacked area would be repaired fast owing to excellent passivation ability of 2205 DSS. When the concentration of HCl solution increases, the attacking of  $\text{Cl}^-$  becomes more severe, while the hydrogen reduction is enhanced. Thus, more defects would appear in the passive film and its stability is apparently reduced in 0.137 mol/L HCl solution (Figure 12b). This is supported by the suddenly drop of pitting potential from 0.75 V to 0.4 V in polarization curve measurement (Figure 1a). Figure 12c shows the corrosion mechanism of 2205 DSS in 0.1 mol/L HCl +  $\text{Na}_2\text{S}$  solution. The adsorption of  $\text{S}^{2-}$  and  $\text{HS}^-$  ions could accelerate the corrosion in some localized areas without passive film protection by promoting the cathodic reaction of hydrogen reduction as indicated by the decrease of charge transfer resistance of electrolyte/metal interface with increasing  $\text{Na}_2\text{S}$  concentration ( $R_2$  of Table 2). On the other hand, most of the surface is under a stable passive film protection which become more stable by adding  $\text{Na}_2\text{S}$  from as evidenced from the increase of film resistance ( $R_1$ ) (Table 2). This phenomenon might be attributed to the competitive adsorption of  $\text{S}^{2-}$  and/or  $\text{HS}^-$  ions to prevent  $\text{Cl}^-$  attacking passive film. However, as more defects exist in the passive film and surface in 0.137 mol/L HCl solution, 2205 DSS is not able to keep stable

passivation when  $N_2S$  reaches 0.385 mmol/L. A significant degradation process is taking place as described in Figure 12d to Figure 12e. The hydrogen reduction and anodic dissolution are significantly accelerated in early stages at localized superficial defects. With more and more hydrogen generation and active dissolution sites expanding, the sample cannot maintain the passivation longer, hence an active dissolution occurred.

As shown in Figure 12e,f, the destruction of passivation can be ascribed to the interaction of  $H_2S$ ,  $HS^-$  ion,  $S^{2-}$  ion,  $H^+$  ion and  $Cl^-$  ion in defects when of hydrochloric acid and  $Na_2S$  concentrations are high enough in the same time. Besides the effect of sulphur species on the adsorption and reduction of hydrogen on metal surface (Figure 11),  $H_2S$ ,  $HS^-$  and  $S^{2-}$  ions adsorbed into surface defect sites of 2205DSS could form FeS intermediate products [51]. Next, the dissolution of FeS in hydrochloric acid produces  $H_2S$  and regeneration of  $H_2S$  facilitates the corrosion of 2205 DSS. When  $H_2S$  and HCl concentrations reach critical values, this process of autocatalysis could accelerate corrosion remarkably - acidic dissolution happens. At the same time of acidic dissolution, the promoted diffusion of H into inside trap at grain boundaries causes a dramatic deterioration in hydrogen induced corrosion resistance. Consequently, grain boundaries are the preferential corrosion site, severely intergranular corrosion between austenite and ferrite phases combined with surficial active dissolution are presented.

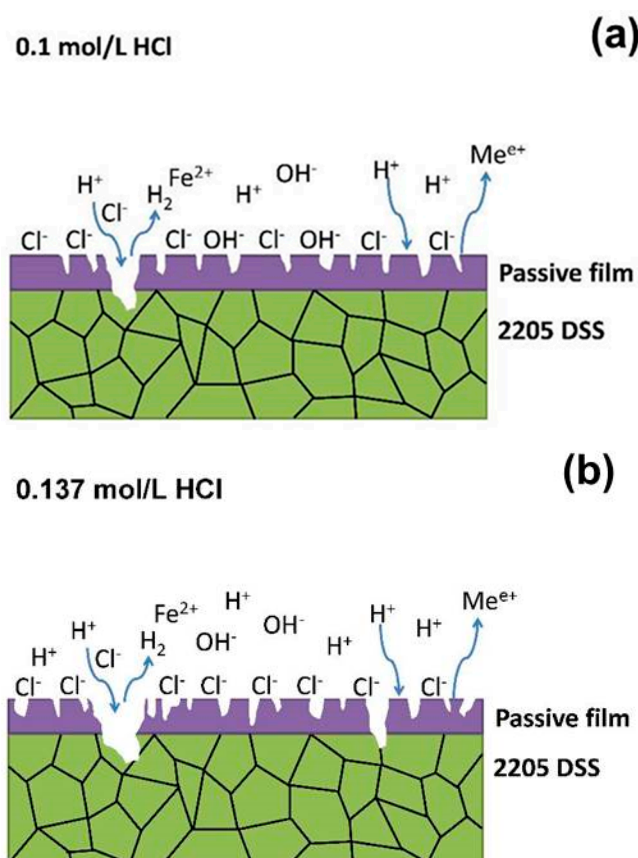
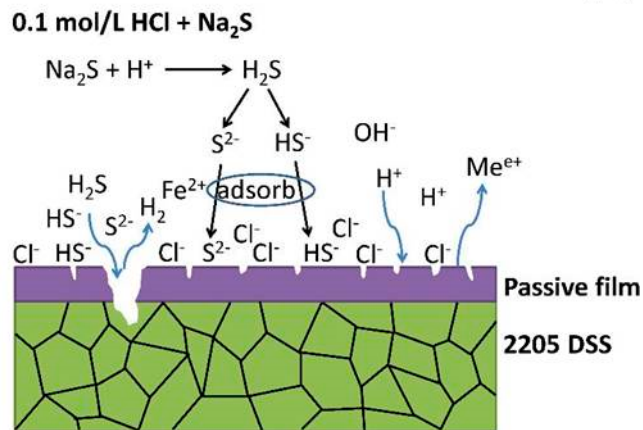
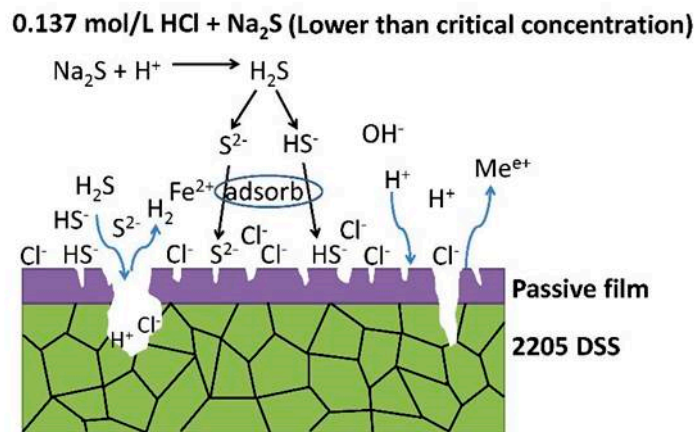


Figure 12. Cont.

(c)



(d)



(e)

**0.137 mol/L HCl + 0.385 mmol/L Na<sub>2</sub>S (Critical concentration)**

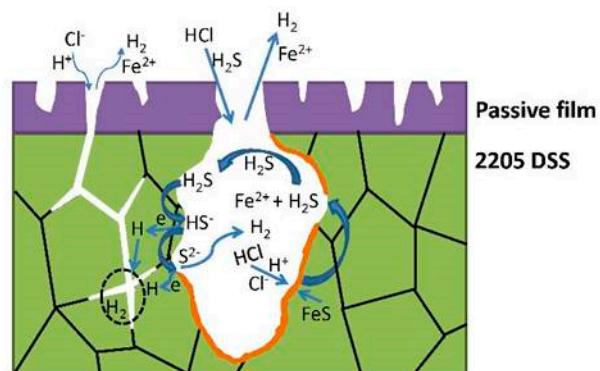
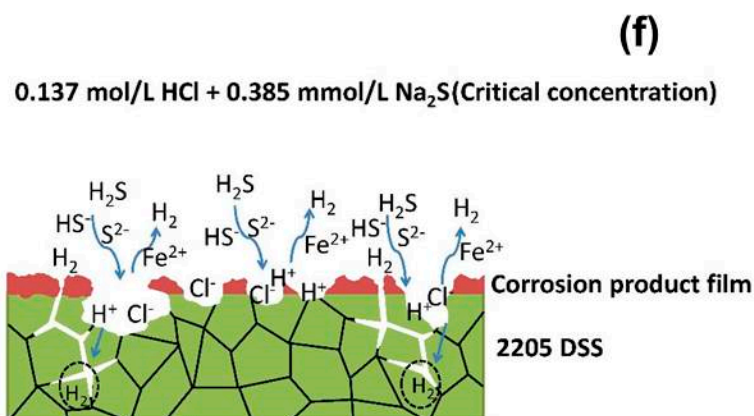


Figure 12. Cont.



**Figure 12.** Corrosion mechanism models of 2205 DSS: (a) 0.1 mol/L HCl, (b) 0.137 mol/L HCl, (c) 0.1 mol/L HCl + Na<sub>2</sub>S, (d) corrosion initiation in 0.137 mol/L HCl + Na<sub>2</sub>S, (e) initiation and propagation of localized defect in 0.137 mol/L HCl + 0.385 mmol/L Na<sub>2</sub>S, (f) corrosion propagation in the entire surface of 2205 DSS in 0.137 mol/L HCl + 0.385 mmol/L Na<sub>2</sub>S

## 5. Conclusions

The corrosion behavior of 2205 DSS in HCl solutions of different concentration with Na<sub>2</sub>S additions at 90 °C were investigated using mass loss, potentiodynamic polarization tests, EIS, SKP, SEM and XPS in this paper and some important points are emphasized as below:

(1) 2205 DSS exhibited high corrosion resistance when HCl concentration was lower than 0.274 mol/L. When 0.385 mmol/L Na<sub>2</sub>S is added in HCl solution of 0.137 mol/L or higher concentration, the corrosion resistance of 2205 DSS would be tremendously reduced and active dissolution happens.

(2) The SKP result showed that the surface potential distribution of 2205 DSS obviously changed after corrosion and the anodic area enlarged. The micromorphology characterization demonstrated that the intergranular corrosion of 2205 DSS could occur in HCl + Na<sub>2</sub>S solution, while it only occurred general corrosion in HCl solution.

(3) The passive film of 2205 DSS in dilute HCl solution with Na<sub>2</sub>S addition is mainly constituted of Cr(III) oxide-hydroxides, which have high chemical stability. Thus, the passive film offers excellent protection for 2205 DSS matrix. In contrast, the corrosion product film formed in active dissolution is mainly composed of metals (except Fe) oxides and/or hydroxides, sulfides, elemental sulphur and chlorides.

(4) HS<sup>-</sup>, S<sup>2-</sup> ions performed high activities of absorption in HCl solutions on 2205 DSS. In 0.1 mol/L HCl solution, competitive absorption between HS<sup>-</sup>, S<sup>2-</sup> and Cl<sup>-</sup> ions would prevent the dissolution of passive film. However, in 0.137 mol/L HCl + 0.385 mmol/L Na<sub>2</sub>S solution, HS<sup>-</sup> and S<sup>2-</sup> ions mainly promoted the process of hydrogen evolution and surface depassivation. The combination effect of H<sup>+</sup>, Cl<sup>-</sup>, HS<sup>-</sup> and S<sup>2-</sup> ions would accelerate the active corrosion remarkably when hydrochloric acid and Na<sub>2</sub>S concentrations are high enough in the same time.

**Author Contributions:** Conceptualization, J.T., H.W. and X.Y.; methodology, J.T., X.Y.; software, Y.X.; validation, J.T., Y.W. and H.W.; formal analysis, X.Y. and Y.W.; investigation, X.Y. and Y.X.; resources, Z.N.; data curation, H.W.; writing—original draft preparation, J.T. and X.Y.; writing—review and editing, H.W., M.A. and B.N.; supervision, B.N.; project administration, H.W.; funding acquisition, H.W.

**Funding:** This research was funded by Scientific Research Innovation Team of Universities Affiliated to Sichuan Province, grant number 18TD0012, Applied Basic Research Programs of Science and Technology Department of Sichuan Province, grant number 2017JY0044 and National Science and Technology Major Project, grant number 2017ZX05030-001.

**Acknowledgments:** The authors thank Zhanfeng He for the scanning Kelvin probe characterization using VersaSCAN system in the State Key Laboratory of Oil and Gas Reservoir Geology and Exploitation, SWPU.

**Conflicts of Interest:** The authors declare no conflict of interest. The funders had no role in the design of the study; in the collection, analyses, or interpretation of data; in the writing of the manuscript, or in the decision to publish the results.

## References

1. Tan, H.; Jiang, Y.; Deng, B.; Sun, T.; Xu, J.; Li, J. Effect of annealing temperature on the pitting corrosion resistance of super duplex stainless steel UNS S32750. *Mater. Charact.* **2009**, *60*, 1049–1054. [[CrossRef](#)]
2. Antony, P.J.; Chongdar, S.; Kumar, P.; Raman, R. Corrosion of 2205 duplex stainless steel in chloride medium containing sulfate-reducing bacteria. *Electrochim. Acta* **2007**, *52*, 3985–3994. [[CrossRef](#)]
3. Kangas, P.; Chai, G.C. Use of advanced austenitic and duplex stainless steels for applications in oil & gas and process industry. *Adv. Mater. Res.* **2013**, *794*, 645–669. [[CrossRef](#)]
4. Huang, B.S.; Yin, W.F.; Sang, D.H.; Jiang, Z.Y. Applied surface science synergy effect of naphthenic acid corrosion and sulfur corrosion in crude oil distillation unit. *Appl. Surf. Sci.* **2012**, *259*, 664–670. [[CrossRef](#)]
5. Cheng, Q.; Tao, B.; Song, L.; Zhang, W.; Liu, X.; Li, W.; Hou, B.; Liu, Q. Corrosion behaviour of Q235B carbon steel in sediment water from crude oil. *Eval. Program Plan.* **2016**, *111*, 61–71. [[CrossRef](#)]
6. Moura, V.; Kina, A.Y.; Tavares, S.S.M.; Lima, L.D.; Mainier, F.B. Influence of stabilization heat treatments on microstructure, hardness and intergranular corrosion resistance of the AISI 321 stainless steel. *J. Mater. Sci.* **2008**, *43*, 536–540. [[CrossRef](#)]
7. Vasconcelos, I.F.; Tavares, S.S.M.; Reis, F.E.U.; Abreu, H.F.G. Ageing effects on  $\alpha'$  precipitation and resistance to corrosion of a novel Cr-Mo stainless steel with high Mo content. *J. Mater. Sci.* **2009**, *44*, 293–299. [[CrossRef](#)]
8. Moiseeva, L.S.; Aisin, A.E. Comparative tests of corrosion inhibitors in simulated media of the Samaraneftgaz oil fields. *Prot. Met.* **2007**, *43*, 84–86. [[CrossRef](#)]
9. Silva, C.C.; Machado, J.P.S.E.; Sobral-Santiago, A.V.C.; de Sant'Ana, H.B.; Farias, J.P. High-temperature hydrogen sulfide corrosion on the heat-affected zone of the AISI 444 stainless steel caused by Venezuelan heavy petroleum. *J. Pet. Sci. Eng.* **2007**, *59*, 219–225. [[CrossRef](#)]
10. Efremov, A.P.; Kim, S.K. Analysis of the corrosion and inhibitive protection of the Lukoil Komi oil-fields equipment. *Prot. Met.* **2006**, *42*, 194–200. [[CrossRef](#)]
11. Mendoza-Canales, J.; Marín-Cruz, J. EIS characterization of corrosion processes of titanium and alloy UNS N10276 in sour environments. *J. Solid State Electrochem.* **2008**, *12*, 1637–1644. [[CrossRef](#)]
12. Jeon, S.-H.; Kim, S.-T.; Lee, J.-S.; Lee, I.-S.; Park, Y.-S. Effects of sulfur addition on the formation of inclusions and the corrosion behavior of super duplex stainless steels in chloride solutions of different pH. *Mater. Trans.* **2012**, *53*, 1617–1626. [[CrossRef](#)]
13. Wan, T.; Xiao, N.; Shen, H.; Yong, X. Ultrasonics Sonochemistry The effect of chloride ions on the corroded surface layer of 00Cr22Ni5Mo3N duplex stainless steel under cavitation. *Ultrason. Sonochem.* **2016**, *33*, 1–9. [[CrossRef](#)] [[PubMed](#)]
14. Chaofang, D.; Hong, L.U.O.; Kui, X.; Ting, S.U.N.; Qian, L.I.U.; Xiaogang, L.I. Effect of temperature and Cl-concentration on pitting of 2205 duplex stainless steel. *J. Wuhan Univ. Technol.* **2011**, *26*, 641–647. [[CrossRef](#)]
15. Lo, I.; Fu, Y.; Lin, C.; Tsai, W. Effect of electrolyte composition on the active-to-passive transition behavior of 2205 duplex stainless steel in H<sub>2</sub>SO<sub>4</sub>/HCl solutions. *Corros. Sci.* **2006**, *48*, 696–708. [[CrossRef](#)]
16. Liu, Z.Y.; Dong, C.F.; Li, X.G.; Zhi, Q.; Cheng, Y.F. Stress corrosion cracking of 2205 duplex stainless steel in H<sub>2</sub>S-CO<sub>2</sub> environment. *J. Mater. Sci.* **2009**, *44*, 4228–4234. [[CrossRef](#)]
17. Liu, R.; Li, J.; Liu, Z.; Du, C.; Dong, C.; Li, X. Effect of pH and H<sub>2</sub>S concentration on sulfide stress corrosion cracking (SSCC) of API 2205 duplex stainless steel. *Int. J. Mater. Res.* **2015**, *106*, 608–613. [[CrossRef](#)]
18. Tranchida, G.; Clesi, M.; di Franco, F.; di Quarto, F.; Santamaria, M. Electronic properties and corrosion resistance of passive films on austenitic and duplex stainless steels. *Electrochim. Acta* **2018**, *273*, 412–423. [[CrossRef](#)]
19. Mohammadi, M.; Choudhary, L.; Gadala, I.M.; Alfantazia, A. Electrochemical and Passive Layer Characterizations of 304L, 316L, and Duplex 2205 Stainless Steels in Thiosulfate Gold Leaching Solutions. *J. Electrochem. Soc.* **2016**, *163*, C883–C894. [[CrossRef](#)]
20. He, W.; Knudsen, O.Ø.; Dıplas, S. Corrosion of stainless steel 316L in simulated formation water environment with CO<sub>2</sub>-H<sub>2</sub>S-Cl<sup>-</sup>. *Corros. Sci.* **2009**, *51*, 2811–2819. [[CrossRef](#)]

21. Veloz, M.A.; Gonza, I. Electrochemical study of carbon steel corrosion in buffered acetic acid solutions with chlorides and H<sub>2</sub>S. *Electrochim. Acta* **2002**, *48*, 135–144. [[CrossRef](#)]
22. Ding, J.; Zhang, L.; Lu, M.; Wang, J.; Wen, Z.; Hao, W. Applied surface science the electrochemical behaviour of 316L austenitic stainless steel in Cl<sup>-</sup> containing environment under different H<sub>2</sub>S partial pressures. *Appl. Surf. Sci.* **2014**, *289*, 33–41. [[CrossRef](#)]
23. Case, R.P.; Rincon, H.E.; McIntyre, D.R. Analysis of pit stability in type 316L stainless steel exposed to H<sub>2</sub>S-saturated dilute chloride solutions above the critical pitting temperature. *Corrosion* **2012**, *68*, 1–12. [[CrossRef](#)]
24. Tang, J.; Hu, Y.; Han, Z.; Wang, H.; Zhu, Y.; Wang, Y.; Nie, Z.; Wang, Y. Experimental and Theoretical Study on the Synergistic Inhibition Effect of Pyridine Derivatives and Sulfur-Containing Compounds on the Corrosion of Carbon Steel in CO<sub>2</sub>-Saturated 3.5 wt.% NaCl Solution. *Molecules* **2018**, *23*, 3270. [[CrossRef](#)] [[PubMed](#)]
25. Yu, L.; Tang, J.; Wang, H.; Wang, Y.; Qiao, J.; Apreutesei, M. Bernard Normand, Corrosion behavior of bulk (Zr<sub>58</sub>Nb<sub>3</sub>Cu<sub>16</sub>Ni<sub>13</sub>Al<sub>10</sub>)<sub>100-x</sub>Y<sub>x</sub> (x = 0, 0.5, 2.5 at.%) metallic glasses in sulfuric acid. *Corros. Sci.* **2019**. [[CrossRef](#)]
26. Marcus, P. Surface science approach of corrosion phenomena. *Electrochim. Acta* **1998**, *43*, 109–118. [[CrossRef](#)]
27. Marcus, P.; Maurice, V.; Strehblow, H.H. Localized corrosion (pitting): A model of passivity breakdown including the role of the oxide layer nanostructure. *Corros. Sci.* **2008**, *50*, 2698–2704. [[CrossRef](#)]
28. Fredriksson, W.; Petrini, D.; Edström, K.; Björefors, F.; Nyholm, L. Corrosion resistances and passivation of powder metallurgical and conventionally cast 316L and 2205 stainless steels. *Corros. Sci.* **2013**, *67*, 268–280. [[CrossRef](#)]
29. Zhang, G.A.; Zeng, Y.; Guo, X.P.; Jiang, F.; Shi, D.Y.; Chen, Z.Y. Electrochemical corrosion behavior of carbon steel under dynamic high pressure H<sub>2</sub>S/CO<sub>2</sub> environment. *Corros. Sci.* **2012**, *65*, 37–47. [[CrossRef](#)]
30. Herbsleb, G.; Poepperling, R.K. Corrosion properties of austenitic-ferritic duplex steel AF 22 in chloride and sulfide containing environments. *Corrosion* **1980**, *36*, 611–618. [[CrossRef](#)]
31. Bhola, S.M.; Bhola, R.; Mishra, B.; Olson, D.L. Povidone-iodine as a corrosion inhibitor towards a low modulus beta Ti-45Nb implant alloy in a simulated body fluid. *J. Mater. Sci. Mater. Med.* **2011**, *22*, 773–779. [[CrossRef](#)] [[PubMed](#)]
32. Bhola, S.M.; Bhola, R.; Mishra, B.; Olson, D.L. Electrochemical impedance spectroscopic characterization of the oxide film formed over low modulus Ti-35.5Nb-7.3Zr-5.7Ta alloy in phosphate buffer saline at various potentials. *J. Mater. Sci.* **2010**, *45*, 6179–6186. [[CrossRef](#)]
33. Qiao, Y.X.; Zheng, Y.G.; Ke, W.; Okafor, P.C. Electrochemical behaviour of high nitrogen stainless steel in acidic solutions. *Corros. Sci.* **2009**, *51*, 979–986. [[CrossRef](#)]
34. Ma, H.; Cheng, X.; Li, G.; Chen, S.; Quan, Z.; Zhao, S.; Niu, L. The influence of hydrogen sulfide on corrosion of iron under different conditions. *Corros. Sci.* **2000**, *42*, 1669–1683. [[CrossRef](#)]
35. Azevedo, C.; Bezerra, P.S.A.; Esteves, F.; Joia, C.J.B.M.; Mattos, O.R. Hydrogen permeation studied by electrochemical techniques. *Electrochim. Acta* **1999**, *44*, 4431–4442. [[CrossRef](#)]
36. Ha, H.Y.; Jang, M.H.; Lee, T.H.; Moon, J. *Understanding the Relation between Phase Fraction and Pitting Corrosion Resistance of UNS 32750 Stainless Steel*; Elsevier B.V.: Amsterdam, The Netherlands, 2015. [[CrossRef](#)]
37. Kittel, J.; Smanio, V.; Fregonese, M.; Garnier, L.; Lefebvre, X. Hydrogen induced cracking (HIC) testing of low alloy steel in sour environment: Impact of time of exposure on the extent of damage. *Corros. Sci.* **2010**, *52*, 1386–1392. [[CrossRef](#)]
38. Sobol, O.; Holzlechner, G.; Nolze, G.; Wirth, T.; Eliezer, D.; Boellinghaus, T.; Wolfgang, E.S. Unger Time-of-Flight Secondary Ion Mass Spectrometry (ToF-SIMS) imaging of deuterium assisted cracking in a 2205 duplex stainless steel microstructure. *Mater. Sci. Eng. A* **2016**, *676*, 271–277. [[CrossRef](#)]
39. Bellezze, T.; Giuliani, G.; Viceré, A.; Roventi, G. Study of stainless steels corrosion in a strong acid mixture. Part 2: Anodic selective dissolution, weight loss and electrochemical impedance spectroscopy tests. *Corros. Sci.* **2018**, *130*, 12–21. [[CrossRef](#)]
40. Femenia, M.; Pan, J.; Leygraf, C.; Luukkonen, P. In situ study of selective dissolution of duplex stainless steel 2205 by electrochemical scanning tunnelling microscopy. *Corros. Sci.* **2001**, *43*, 1939–1951. [[CrossRef](#)]
41. Luo, H.; Dong, C.F.; Xiao, K.; Li, X.G. Characterization of passive film on 2205 duplex stainless steel in sodium thiosulphate solution. *Appl. Surf. Sci.* **2011**, *258*, 631–639. [[CrossRef](#)]
42. Liu, C.T.; Wu, J.K. Influence of pH on the passivation behavior of 254SMO stainless steel in 3.5% NaCl solution. *Corros. Sci.* **2007**, *49*, 2198–2209. [[CrossRef](#)]

43. Sun, W.; Nestic, S. A mechanistic model of H<sub>2</sub>S corrosion of mild steel. In Proceedings of the NACE Proceedings, Nashville, TN, USA, 11–15 March 2007.
44. Tang, J.; Shao, Y.; Guo, J.; Zhang, T.; Meng, G.; Wang, F. The effect of H<sub>2</sub>S concentration on the corrosion behavior of carbon steel at 90 °C. *Corros. Sci.* **2010**, *52*, 2050–2058. [[CrossRef](#)]
45. Zimer, A.M.; Rios, E.C.; Mendes, P.D.; Gonçalves, W.N.; Bruno, O.M.; Pereira, E.C.; Mascaro, L.H. Investigation of AISI 1040 steel corrosion in H<sub>2</sub>S solution containing chloride ions by digital image processing coupled with electrochemical techniques. *Corros. Sci.* **2011**, *53*, 3193–3201. [[CrossRef](#)]
46. Shoesmith, D.W.; Bailey, M.G.; Ikeda, B. Electrochemical formation of mackinawite in alkaline sulphide solutions. *Electrochim. Acta* **1978**, *23*, 1329–1339. [[CrossRef](#)]
47. Tiwari, G.P.; Bose, A.; Chakravartty, J.K.; Wadekar, S.L.; Totlani, M.K.; Arya, R.N.; Fotedar, R.K. A study of internal hydrogen embrittlement of steels. *Mater. Sci. Eng. A* **2000**, *286*, 269–281. [[CrossRef](#)]
48. González, J.; Gutiérrez-Solana, F.; Varona, J.M. The effects of microstructure, strength level, and crack propagation mode on stress corrosion cracking behavior of 4135 steel. *Metall. Mater. Trans. A* **1996**, *27*, 281–290. [[CrossRef](#)]
49. Sozańska, M.; Kłyk-Spyra, K. Investigation of hydrogen induced cracking in 2205 duplex stainless steel in wet H<sub>2</sub>S environments after isothermal treatment at 675, 750 and 900 °C. *Mater. Charact.* **2006**, *56*, 399–404. [[CrossRef](#)]
50. Sobol, O.; Nolze, G.; Saliwan-Neumann, R.; Eliezer, D.; Boellinghaus, T.; Unger, W.E. Novel approach to image hydrogen distribution and related phase transformation in duplex stainless steels at the sub-micron scale. *Int. J. Hydrogen Energy* **2017**, *42*, 25114–25120. [[CrossRef](#)]
51. Mancia, F. The effect of environmental modification on the sulphide stress corrosion cracking resistance of 13Cr martensitic stainless steel in H<sub>2</sub>S-CO<sub>2</sub>-Cl-systems. *Corros. Sci.* **1987**, *27*, 1225–1237. [[CrossRef](#)]



© 2019 by the authors. Licensee MDPI, Basel, Switzerland. This article is an open access article distributed under the terms and conditions of the Creative Commons Attribution (CC BY) license (<http://creativecommons.org/licenses/by/4.0/>).